Dual leucine zipper kinase is required for excitotoxicity-induced neuronal degeneration

Christine D. Pozniak,[1] Arundhati Sengupta Ghosh,[1] Alvin Gogineni,[2] Jesse E. Hanson,[1] Seung-Hye Lee,[1] Jessica L. Larson,[3] Hilda Solanoy,[1] Daisy Bustos,[4] Hong Li,[4] Hai Ngu,[5] Adrian M. Jubb,[5] Gai Ayalon,[1] Jiansheng Wu,[4] Kimberly Scearce-Levie,[1] Qiang Zhou,[1] Robby M. Weimer,[1,2] Donald S. Kirkpatrick,[4] and Joseph W. Lewcock[1]

[1]Department of Neuroscience, [2]Department of Biomedical Imaging, [3]Department of Bioinformatics and Computational Biology, [4]Department of Protein Chemistry, [5]Department of Pathology, Genentech, Inc., South San Francisco, CA 94080

Excessive glutamate signaling is thought to underlie neurodegeneration in multiple contexts, yet the pro-degenerative signaling pathways downstream of glutamate receptor activation are not well defined. We show that dual leucine zipper kinase (DLK) is essential for excitotoxicity-induced degeneration of neurons in vivo. In mature neurons, DLK is present in the synapse and interacts with multiple known postsynaptic density proteins including the scaffolding protein PSD-95. To examine DLK function in the adult, DLK-inducible knockout mice were generated through Tamoxifen-induced activation of Cre-ERT in mice containing a floxed *DLK* allele, which circumvents the neonatal lethality associated with germline deletion. DLK-inducible knockouts displayed a modest increase in basal synaptic transmission but had an attenuation of the JNK/c-Jun stress response pathway activation and significantly reduced neuronal degeneration after kainic acid–induced seizures. Together, these data demonstrate that DLK is a critical upstream regulator of JNK-mediated neurodegeneration downstream of glutamate receptor hyper-activation and represents an attractive target for the treatment of indications where excitotoxicity is a primary driver of neuronal loss.

CORRESPONDENCE
Joseph W. Lewcock:
lewcock.joseph@gene.com

Abbreviations used: DRG, dorsal root ganglion; EPSP, excitatory postsynaptic potential; LTP, long-term potentiation; NMDA, *N*-methyl D-aspartate.

Glutamate-based excitotoxicity is thought to underlie much of the neuronal damage that occurs after stroke or traumatic brain injury and contributes to functional decline in neurodegenerative disorders such as amyotrophic lateral sclerosis (ALS) and Alzheimer's disease (Hardingham and Bading, 2010; Lau and Tymianski, 2010). An excess of extracellular glutamate present as a result of trauma or disease leads to hyper-activation of ionotrophic glutamate receptors, causing high levels of calcium influx into affected neurons that eventually results in degeneration (Choi, 1985). The *N*-methyl D-aspartate (NMDA) receptor has been shown to be a primary mediator of excitotoxicity-induced neuronal cell death, and treatment with NMDA receptor-specific antagonists is neuroprotective in several degeneration models (Simon et al., 1984;Virgili et al., 1992).

Uncoupling of NMDA receptors from the associated scaffolding protein PSD-95 can protect neurons from excitotoxic degeneration, suggesting that an interaction with intracellular signaling molecules is required to initiate a pro-apoptotic response (Aarts et al., 2002; Cook et al., 2012). In particular, the JNK pathway has emerged as an important regulator of neuronal degeneration induced by NMDA receptor hyper-activation. Inhibitors of JNK activity can prevent both NMDA-mediated neuronal apoptosis in vitro and after ischemia in vivo (Borsello et al., 2003; Gao et al., 2005). Additionally, significant neuroprotection from kainic acid–induced excitotoxicity was observed in mice lacking expression of JNK3 or expressing a mutated form of the downstream transcription factor c-Jun that cannot be phosphorylated by JNK (Yang et al., 1997; Behrens et al., 1999). However, despite extensive data supporting a role for JNK in excitotoxic neurodegeneration,

The Rockefeller University Press $30.00
J. Exp. Med. 2013 Vol. 210 No. 12 2553-2567
www.jem.org/cgi/doi/10.1084/jem.20122832

The Journal of Experimental Medicine

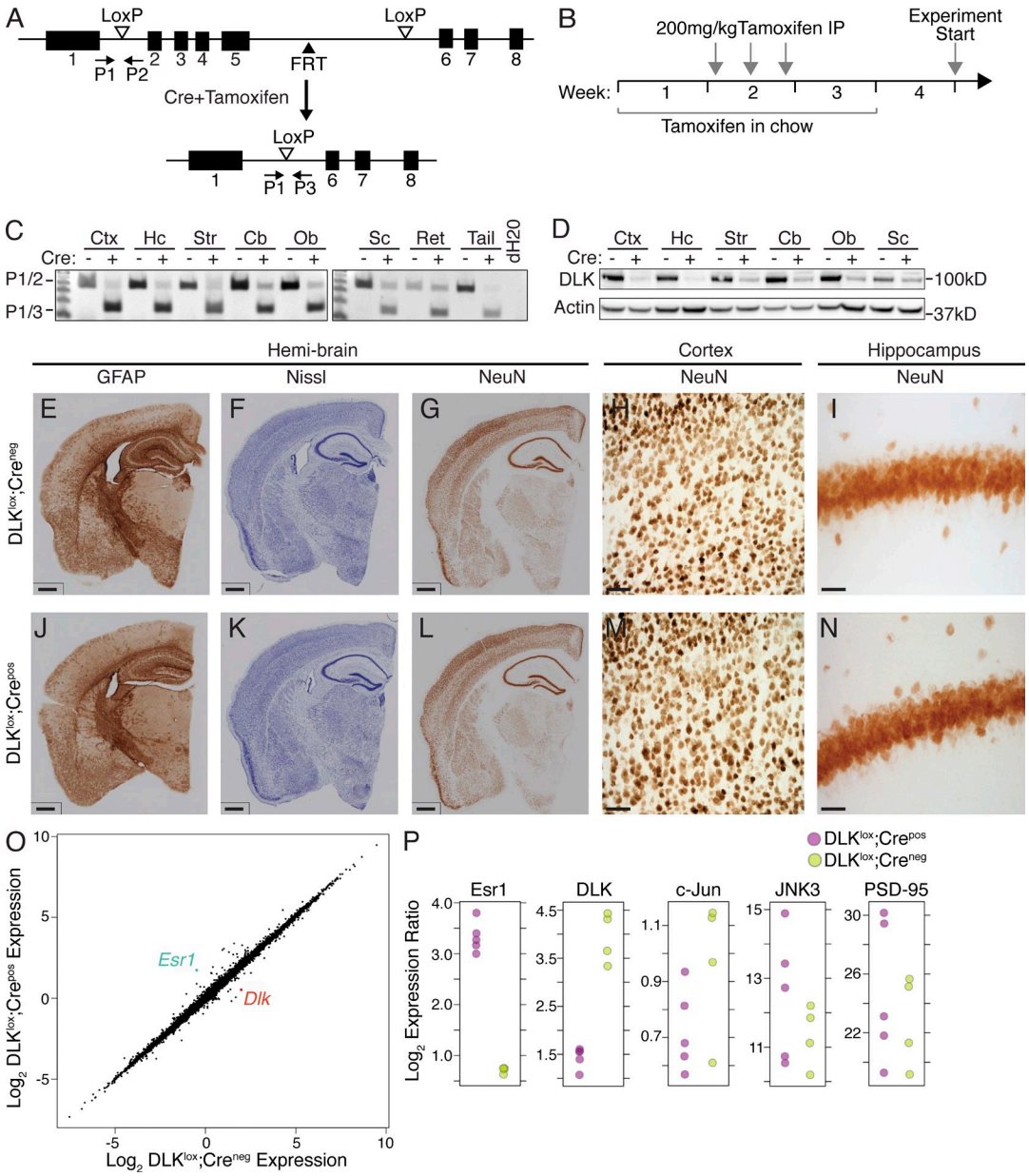

Figure 1. Generation and characterization of DLK-inducible knockout mice. (A) Schematic of the strategy used to generate DLK-inducible knockout mice. DLK^{lox} mice were crossed to CAG-CreERT mice to generate DLK^{lox};Cre^{pos} mice. Tamoxifen exposure resulted in excision of *DLK* exons 2–5. P1, P2, and P3 represent primers used for analysis of recombination. (B) Experimental design for *DLK* excision in the adult DLK^{lox};Cre^{pos} animals. Mice were fed Tamoxifen chow for 3 wk and received three Tamoxifen injections (i.p.) during week 2 before initiating studies at the end of week 4. (C) Genomic DNA PCR from the CNS of Tamoxifen-treated DLK^{lox};Cre^{pos} or DLK^{lox};Cre^{neg} mice. Cre genotype is annotated by a + or − symbol. The upper band (263 bp) corresponds to full-length unrecombined *DLK* (P1+P2), whereas the lower band (150 bp) is the product of *DLK* recombination in DLK^{lox};Cre^{pos} mice (P1+P3). Data are representative of $n > 10$ mice per genotype. Ctx = cortex, Hc = hippocampus, Str = striatum, Cb = cerebellum, Ob = olfactory bulb, Sc = spinal cord, Ret = retina. (D) Western blot analysis of DLK protein in various regions of the CNS in DLK^{lox};Cre^{pos} and DLK^{lox};Cre^{neg} mice. Cre genotype is annotated by a + or − symbol and Actin is shown as a loading control. Data are representative of $n = 5$ mice per genotype. Ctx = cortex, Hc = hippocampus, Str = striatum, Cb = cerebellum, Ob = olfactory bulb, Sc = spinal cord. (E–N) Immunohistochemistry for GFAP (E and J), Nissl stain (F and K), and NeuN (G and L) on hemibrains from DLK^{lox};Cre^{neg} (top) and DLK^{lox};Cre^{pos} mice (bottom). Bars, 300 µm. High magnification images of cortex (H and M) and hippocampus (I and N) of Tamoxifen-treated DLK^{lox};Cre^{neg} or DLK^{lox};Cre^{pos} mice after NeuN staining. Bars: (E–G and J–L) 300 µm; (H and M) 50 µm; (I and N) 30 µm. Data are representative of $n \geq 5$ mice per genotype. (O) Mean $\log_2$ normalized expression for all genes in the microarray experiment is plotted for DLK^{lox};Cre^{neg} samples (x-axis) and DLK^{lox};Cre^{pos} samples (y-axis). Significantly different genes are highlighted in red (*Dlk*) and blue (*Esr1*; $P \leq 0.01$ for both genes). $n = 4$ animals for DLK^{lox};Cre^{neg} and 5 for DLK^{lox};Cre^{pos}. (P) *Esr1*, *DLK*, *c-Jun*, *JNK3*, *and PSD-95* expression levels from microarray in DLK^{lox};Cre^{pos} samples (purple) as compared with DLK^{lox};Cre^{neg} controls (yellow). The y-axis was set based on the maximum and minimum expression observed in individual animals and differs for each gene shown. $n = 4$ animals for DLK^{lox};Cre^{neg} and 5 for DLK^{lox};Cre^{pos}.

Table 1. DLK-interacting proteins identified by mass spectrometry

Gene	Uniprot Symbol	Present in PSD	Peptides in DLK^{lox}:Cre^{neg}	Peptides in DLK^{lox}:Cre^{pos}
DLK	MAP3K12	X	23	1
Beta spectrin 2	Spnb2	X	28	0
LZK	MAP3K13		13	0
Neurofilament light	Nefl	X	13	0
Neurofilament medium	Nefm	X	12	0
Beta spectrin 3	Spnb3	X	10	0
Internexin	Ina	X	9	0
Matrin 3	Matr3		7	0
Purine rich binding protein element A	Pura	X	7	0
Microtubule associate protein 1A	Map1a	X	6	0
Contactin 1	Cntn1	X	5	0
Actinin alpha 1	Actn1	X	5	0
DEAH box polypeptide 9	Dhx9		5	0
Synaptic RAS GTPase activating protein	Syngap1	X	4	0
Microtubule associate protein 4	Map4	X	4	0
Heterogeneous nuclear ribonucleoprotein a2b1	HNRPa2b1		4	0
BR serine/threonine kinase 1	Brsk1		4	0
PSD-95	DLG4	X	3	0
Set binding factor 1	sbf1	X	3	0
Kinesin family member 2A	Kif2	X	2	0

"Present in PSD" denotes peptides identified in PSD fraction after biochemical fractionation. All peptides except DLK and Map4 have been identified in multiple independent studies.

the upstream factors that link JNK to glutamate receptor hyper-activation remain poorly understood.

Dual leucine zipper kinase (DLK) is an evolutionarily conserved mixed lineage kinase that is required for stress-induced JNK activity in neurons during development (Ghosh et al., 2011) and is essential for both neurodegeneration and axon regeneration of dorsal root ganglion (DRG) and retinal ganglion cell neurons after insult (Miller et al., 2009; Ghosh et al., 2011; Shin et al., 2012; Watkins et al., 2013). These findings, together with the localization of DLK protein to the axon (Hirai et al., 2005; Lewcock et al., 2007), have led to the hypothesis that DLK acts as a damage sensor to control the neuronal response to axonal injury. High levels of DLK expression can be found throughout the adult brain (Mata et al., 1996), yet the function of DLK outside of these specific populations of projection neurons remains unclear. In this study, we performed an unbiased analysis of DLK-interacting proteins in the adult brain and found that DLK is present at the postsynaptic density and can interact with many PSD components, including PSD-95 in mature neurons. Removal of DLK in adult animals provided significant protection of neurons from excitotoxicity-induced degeneration via attenuation of stress-induced JNK signaling. These results represent a novel role for DLK in the response to neuronal insult originating at the synapse and suggest that DLK may broadly regulate neurodegeneration in the adult brain.

RESULTS

To investigate the role of DLK in the adult brain, we generated mice in which excision of the DLK allele can be temporally controlled to avoid the lethality observed at early postnatal ages in DLK-null mice (Hirai et al., 2006). This was achieved by crossing mice with DLK exons 2–5 flanked by loxP sites (DLK$^{lox/lox}$) to a Tamoxifen-inducible Cre-ERT transgene driven by the CMV early enhancer/chicken β actin (CAG) promoter (Fig. 1 A) that expresses high levels of Cre-ERT in brain and most peripheral tissues (Hayashi and McMahon, 2002). DLK$^{lox/lox}$/Cre-ERT^{pos} mice (referred to as DLK^{lox};Cre^{pos}) displayed minimal recombination of the *DLK* allele in the absence of Tamoxifen and survived to adulthood. To induce *DLK* recombination, 10–12-wk-old DLK^{lox};Cre^{pos} mice were put on a Tamoxifen diet for 3 wk combined with three high-dose injections of Tamoxifen (Fig. 1 B), which resulted in efficient excision of DLK in most brain regions (Fig. 1 C). Although the vast majority of DLK protein was eliminated in many brain regions 1 wk after completion of Tamoxifen dosing, a small amount of DLK protein was still present, consistent with the levels of unrecombined *DLK* observed by PCR in each brain region (Fig. 1, C and D). Nonetheless, this dosing regimen achieved a reduction in DLK levels that was adequate to assess the function of this kinase in the adult CNS and thus avoid confounding developmental phenotypes.

The effect of *DLK* deletion in DLK^{lox};Cre^{pos} brains was first assessed by histological analysis of animals after Tamoxifen administration, which identified no gross abnormalities as compared with control littermates lacking Cre expression (Fig. 1, E–N). NeuN staining (Fig. 1, I and N) of brains of both genotypes revealed normal morphology and organization of neurons in the cortex and hippocampus. To examine what changes in gene expression resulted from Tamoxifen-induced excision of *DLK*, we performed microarray analysis on the hippocampi

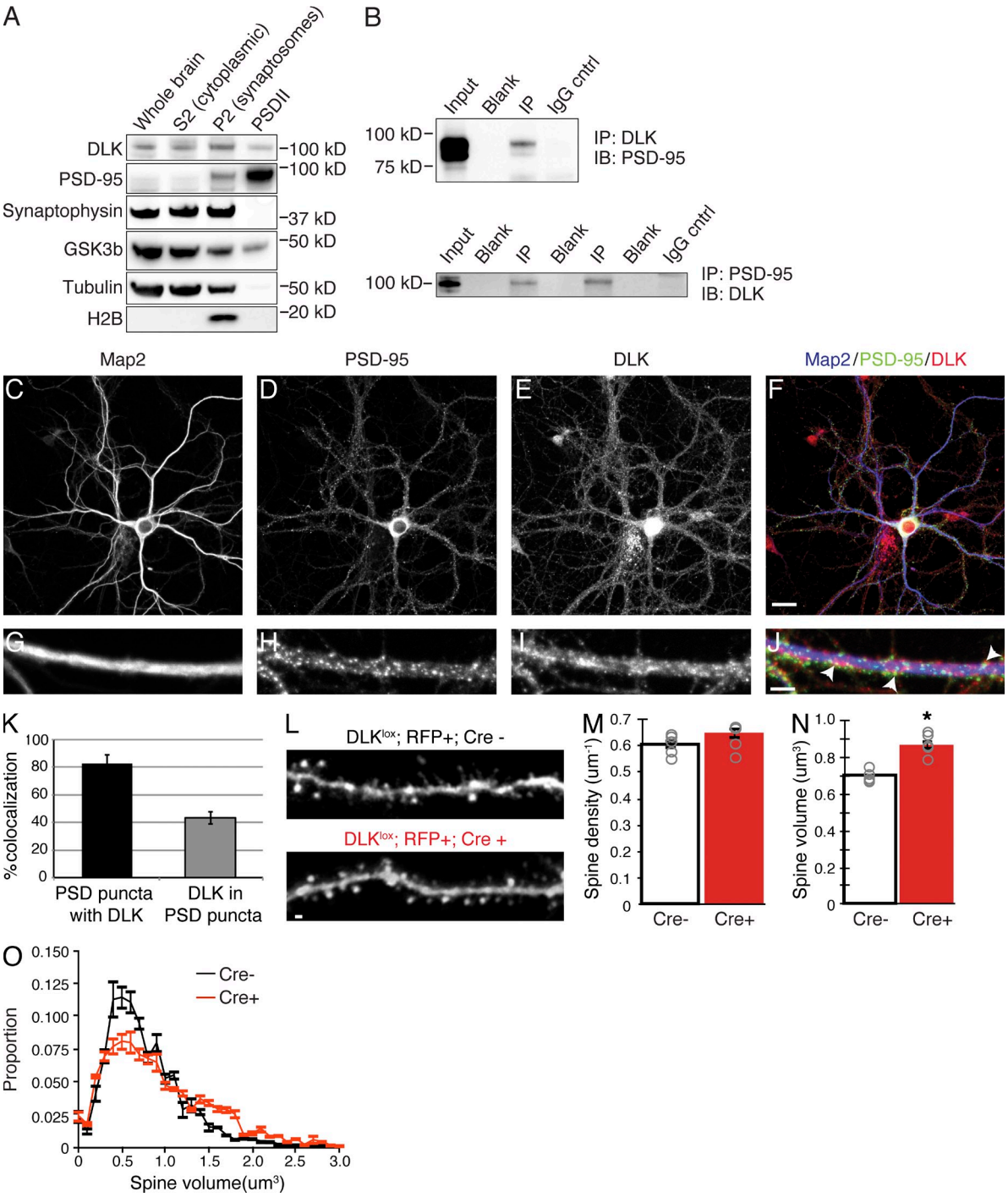

Figure 2. DLK is present in the postsynaptic density and associates with PSD-95. (A) Western blot of adult rat brain fractionated to isolate the postsynaptic density blotted with antibodies to DLK, PSD-95, synaptophysin, GSK3β, tubulin, and histone 2B (H2B). P2 = crude synaptosome proteins, PSDI = synaptosome proteins, and PSDII = core PSD proteins. Data are representative of three independent experiments. (B) Immunoprecipitation (IP) with antibodies for DLK from adult rat brain followed by blotting for PSD-95 (top) or IP with PSD-95 followed by blotting for DLK (bottom). A nonspecific IgG antibody was used as a negative control. Molecular masses are in kilodaltons. Data are representative of at least three independent experiments. (C–J) Confocal images of mature rat hippocampal cultures (21 DIV) stained with Map2 (C), PSD-95 (D), and DLK (E). Merged images are shown in F. In the merged image, DLK is shown in red, PSD-95 in green, and Map2 in blue. Data are representative of $n \geq 5$ cells from three independent experiments. Bar, 30 µm. (G–J) High magnification images of dendrites from neurons in C–J stained with Map2 (G), PSD-95 (H), and DLK (I). Merged image is shown in J. In the merged image, DLK is shown in red, PSD-95 in green, and Map2 in blue. Arrowheads highlight areas of colocalization between DLK and PSD-95. Bar, 10 µm. (K) Quantification of colocalization between PSD-95 and DLK along mature hippocampal dendrites based on $n \geq 15$ cells from three independent experiments. 83 ± 6.1% of PSD-95 positive puncta also contained DLK signal, whereas 43 ± 4.4% of DLK-positive puncta contained PSD-95.

of Tamoxifen-treated DLK^{lox};Cre^{pos} and DLK^{lox};Cre^{neg} age-matched controls. The genetic profiles of the two groups were strikingly similar, including genes potentially involved in DLK signaling such as *c-Jun*, *JNK3*, and *PSD-95*. Surprisingly, the only genes that displayed a significant difference in expression identified between groups were *estrogen receptor α* (*Esr1*) and *DLK* (Fig. 1, O and P). The expression change observed in *Esr1* was expected as a result of the estrogen response element present in the Cre-ER transgene and thus represented a useful internal control for the experiment. Consistent with these findings, observation of DLK^{lox};Cre^{pos} animals for 3 mo after Tamoxifen treatment revealed no changes in body weight or decreased viability as a result of the reduced DLK expression. Together, these data suggest that deletion of *DLK* in the adult brain does not result in similar phenotypes to those observed in germline DLK-null animals (Hirai et al., 2006).

DLK is present at the postsynaptic density and interacts with PSD-95

To better define the role of DLK in the adult brain, we performed a mass spectrometry–based screen for DLK-interacting proteins. DLK protein complexes were immunoprecipitated from whole brains of ∼15-wk-old DLK^{lox};Cre^{neg} animals with an antibody directed against the C terminus of DLK, and then immunoprecipitated protein complexes were subsequently separated by SDS-PAGE and a series of regions spanning the length of the gel were subjected to tryptic digestion and mass spectrometry analysis (see Materials and methods). Immunoprecipitation from brains of Tamoxifen-treated DLK^{lox};Cre^{pos} animals with significantly reduced DLK expression were used as controls to ensure the interacting proteins identified were DLK dependent. Although DLK^{lox};Cre^{pos} mice did retain very low levels of DLK protein (Fig. 1 D) and one peptide corresponding to DLK was identified by mass spectrometry in these animals after immunoprecipitation (Table 1), we restricted our analysis to peptides that were specific to the DLK^{lox};Cre^{neg} condition (i.e., no peptides identified in DLK^{lox};Cre^{pos} animals) to ensure any proteins identified were true components of a DLK protein complex.

Several DLK-interacting proteins were discovered through this analysis, including the closely related mixed lineage kinase LZK (MAP3K13) and several components of the neuronal cytoskeleton such as β spectrin (Spnb2), neurofilament light (Nefl), neurofilament medium (Nefm), and microtubule-associated protein 1a (Map1a; Table 1). Additional DLK-specific interactors included proteins with known roles in synaptic development/function such as contactin 1 (Cntn1; Murai et al., 2002), synaptic Ras GTPase (Syngap1; Kim et al., 1998), and PSD-95 (Sampedro et al., 1981). PSD-95 localization is restricted to the postsynaptic density of mature neurons where it acts as an essential regulator of proper synaptic function (Migaud et al., 1998), and the identification of PSD-95 in our unbiased screen suggests that at least a subset of DLK protein may also be present at the synapse. Indeed, further analysis revealed that a majority of the DLK interactors found here have previously been identified as PSD components by independent mass spectrometry studies which used biochemical fractionation to isolate the postsynaptic density (Table 1; Walikonis et al., 2000; Jordan et al., 2004; Li et al., 2004; Peng et al., 2004; Yoshimura et al., 2004; Collins et al., 2006), and a subset of these studies also identified DLK as a component of the PSD. This observation, along with the interaction observed between DLK and multiple known PSD proteins, suggests that DLK may be present at synapses.

We next sought to more conclusively validate the presence of DLK in the postsynaptic density using several approaches. First, the PSD was isolated by biochemical fractionation to examine whether DLK protein was a component in the enriched PSDII fraction comprised of only core PSD proteins. We observed DLK in the PSDII fraction, while three controls (synaptophysin, tubulin, and histone H2B) known to be absent from the PSD were not present (Fig. 2 A). The lack of enrichment for DLK in the PSDII fraction indicates that DLK protein is not exclusively localized to the PSD and is also present in other subcellular domains. This distribution is common for many previously identified components of the PSD such as GSK3β (Fig. 2 A; Collins et al., 2006). We next performed coimmunoprecipitation of DLK and PSD-95 from adult rat brain to confirm the interaction observed by mass spectrometry. An interaction between these proteins was observed when using either DLK or PSD-95 for pulldown, although immunoprecipitation with DLK pulled down only a fraction of PSD-95, consistent with our biochemical results (Fig. 2 B). Last, immunohistochemistry was performed on mature hippocampal neuron cultures, which revealed punctate DLK staining in MAP2-positive dendrites that colocalized with PSD-95 in some regions of the dendrite (Fig. 2, C–J). The specificity of the DLK antibody was confirmed through staining of neurons from DLK-null mice, in which the punctate DLK staining in neurites was not observed. Staining of cell bodies still occurred in neurons lacking DLK expression, suggesting nonspecific labeling in this region of the neuron (not depicted; Ghosh et al., 2011). Automated quantification of PSD-95 and DLK colocalization along dendrites revealed that the significant majority (83%) of PSD-95–positive puncta contained DLK, whereas only 43% of the total DLK was localized within

Error bars represent SD. (L) Representative fluorescent micrographs of apical dendrite segments from neurons electroporated with an RFP-expressing plasmid (top) and both RFP- and Cre-expressing plasmids (bottom) in DLK^{lox} animals. Bar, 1 µm. (M and N) Quantification of the mean spine density and relative spine volume from Cre-negative versus Cre-positive DLK^{lox} neurons labeled with RFP. Bar graph represents the mean across animals per group and gray circles represent average measures from individual animals, **, $P < 0.01$, unpaired Student's *t* test, $n = 5$ animals, 31 cells, 1,522 spines for Cre-negative and 6, 34 and 1,799 for Cre-positive groups. Error bars represent SEM. (O) Mean frequency distribution of spine volumes for experiments shown in L–N, binned in 0.1-µm^3 increments per animal and averaged across each group. Error bars represent SEM per volume bin per group.

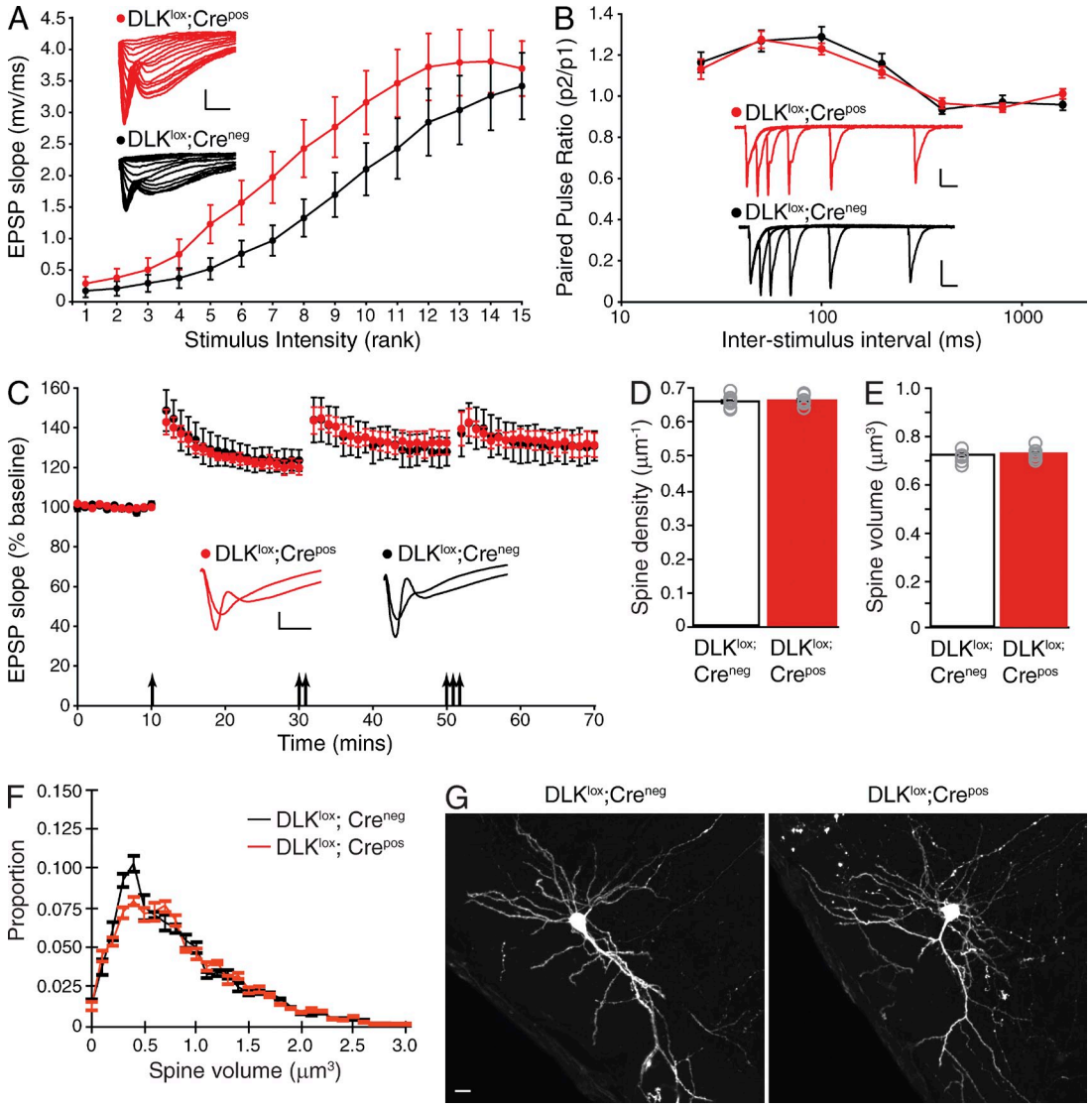

Figure 3. Assessment of neuronal morphology and synaptic activity in DLK-inducible knockout mice. (A) Quantification of EPSP magnitude in response to logarithmically increasing stimulus strengths for DLK^{lox};Cre^{pos} compared with DLK^{lox};Cre^{neg} animals ($P < 0.001$, $n = 18$ individual recordings for DLK^{lox};Cre^{pos} and 19 for DLK^{lox};Cre^{neg}). Example responses for each genotype are shown inset with the scale bar representing 1 mV and 5 ms. (B) Quantification of paired pulse ratios (PPRs) for EPSPs elicited at 25, 50, 100, 200, 400, 800, or 1,600 ms interstimulus interval in both genotypes ($n = 18$ individual recordings for DLK^{lox};Cre^{pos} and 19 for DLK^{lox};Cre^{neg}). Example overlaid EPSP recordings from each genotype for the 25–400-ms intervals are shown inset for each genotype with scale bars representing 1 mV and 20 ms. (C) LTP measurements in slices from DLK^{lox};Cre^{pos} and DLK^{lox};Cre^{neg} mice after sequential bouts of 1, 2, or 3× theta burst stimulation (TBS, indicated by arrows). $n = 6$ individual recordings for DLK^{lox};Cre^{pos} and 7 for DLK^{lox};Cre^{neg}. Example traces from each genotype for the baseline period and after the 3× TBS are shown inset with the scale bar representing 1 mV and 5 ms. Error bars in A–C represent SEM. (D and E) Quantification of mean spine density and relative spine volume in GFP labeled neurons from DLK^{lox};Cre^{neg} and DLK^{lox};Cre^{pos} mice after tamoxifen-induced recombination in the adult animal. Bar graphs represent the mean across animals per group and gray circles represent average measures from individual animals. P-values calculated from unpaired Student's *t* test ($P = 0.8$), $n = 7$ animals, 42 cells, 2,643 spines for DLK^{lox};Cre^{neg} and 7, 45, and 2,699, respectively, for DLK^{lox};Cre^{pos} groups. Error bars represent SEM. (F) Mean frequency distribution of spine volumes for experiment shown in D and E, binned in 0.1-µm^3 increments per animal, and averaged across each group. Error bars represent SEM per volume bin per group. (G) Whole mount images of GFP-labeled cortical neurons from adult DLK^{lox};Cre^{neg} or DLK^{lox};Cre^{pos} mice. Bar, 30 µm. Images are representative of $n = 5$ neurons from at least three animals.

PSD-95–positive regions. Collectively, these data demonstrate that although DLK is not restricted to the postsynaptic density, some DLK protein is present at the PSD and can interact with PSD-95.

To explore whether DLK signaling has a functional role at postsynaptic sites, we assessed the density and size of dendritic spines in pyramidal neurons lacking DLK. As spine density in cultured neurons can be variable, we examined spine morphology in vivo using in utero electroporation of DLK^{lox};Cre^{neg} embryonic day 16.5 (E16.5) mice with Cre-expressing plasmids to allow for examination of cell-autonomous DLK-dependent alterations in neuronal morphology (Saito and Nakatsuji, 2001).

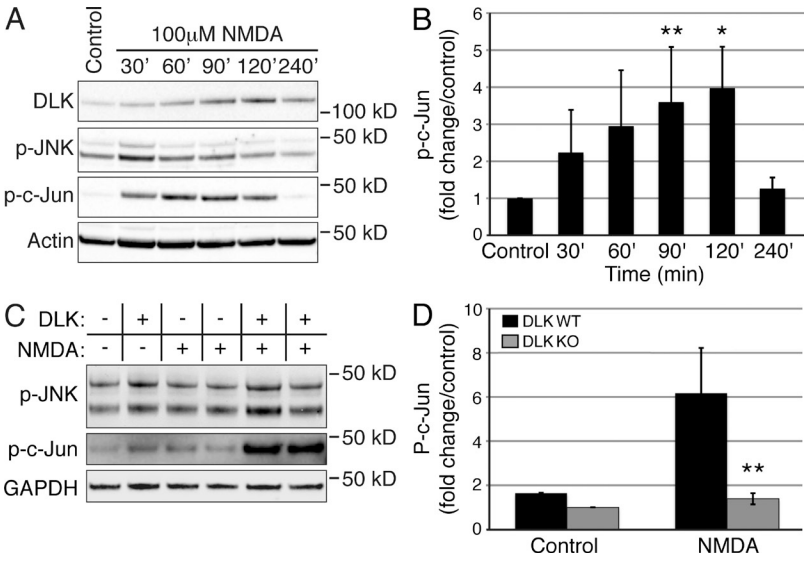

Figure 4. DLK-null neurons display attenuated JNK activation after NMDA treatment. (A) Western blots for DLK, p-JNK, and p-c-Jun of lysates from hippocampal neurons (21–28 DIV) treated with NMDA for 30, 60, 90, 120, or 240 min. Actin is shown as a loading control. (B) Quantification of p-c-Jun levels in NMDA treated hippocampal neurons shown in (A). $n = 6$ independent experiments; **, $P < 0.01$ and *, $P = 0.025$ as determined by an unpaired Student's *t* test. Error bars represent SEM. (C) Western blots for p-c-Jun and p-JNK from DLK WT and KO cortical neurons (14 DIV) treated with NMDA for 60 min. GAPDH is shown as a loading control. (D) Quantification of p-c-Jun protein levels in NMDA-treated DLK WT versus KO neurons shown in (C). $n = 6$ total samples from three independent experiments. **, $P < 0.01$; error bars represent SEM.

When two independent cohorts were assessed at postnatal day 30, loss of DLK did not result in alterations in dendritic spine density along apical dendrites (Fig. 2, L and M), but mean spine volume was increased (Fig. 2 N). Further analysis of spine volume distribution in Cre^{-} versus Cre^{+} neurons revealed that the increase in mean spine volume was the result of an increase in the number of medium spines at the expense of smaller sized spines, with the population of large spines being relatively unaffected (Fig. 2 O). These data suggest that DLK has a functional role at the synapse; however, it is unclear whether the spine size increase is a result of alterations in synaptic development or maintenance.

DLK affects synaptic strength in the adult brain

The DLK-dependent change in spine size led us to ask whether synaptic activity was altered in adult DLK^{lox};Cre^{pos} mice after Tamoxifen-induced deletion of *DLK*. To assess basal synaptic strength, the input-output relationship was determined by measuring excitatory postsynaptic potential (EPSP) magnitude in pyramidal neurons in response to logarithmically increasing stimulus strengths in hippocampi of DLK^{lox};Cre^{neg} versus DLK^{lox};Cre^{pos} animals 1 wk after Tamoxifen treatment. Interestingly, DLK^{lox};Cre^{pos} animals had a modest but significant increase in basal synaptic strength as compared with DLK^{lox};Cre^{neg} age-matched controls ($P < 0.001$, $n = 18$ or 19 recordings, Fig. 3 A). To determine whether this increase in amplitude was a result of presynaptic function, we next examined the paired pulse ratios of EPSPs at several interstimulus intervals. No significant difference in presynaptic strength was observed between genotypes (Fig. 3 B), suggesting that the observed alterations in synaptic strength were postsynaptic in origin. Examination of synaptic plasticity revealed no change in the magnitude of long-term potentiation (LTP) in DLK^{lox};Cre^{pos} versus DLK^{lox};Cre^{neg} mice (Fig. 3 C).

We then asked whether Tamoxifen-induced excision of *DLK* in the adult brain affected spine density or volume similar to what we observed in neurons when DLK was removed during embryonic development (Fig. 2, N and O). To test this, brains of E16.5 embryos from DLK^{lox};Cre^{neg} or DLK^{lox};Cre^{pos} mice were electroporated with GFP and Cre reporter plasmids, treated with Tamoxifen in adulthood to recombine *DLK* in Cre^{pos} animals, and imaged 1 wk later. In this experimental paradigm, DLK deletion in adult neurons did not significantly affect spine density or volume (Fig. 3, D and F), possibly due to reduced plasticity and the slow rate of spine turnover in the adult brain (Holtmaat et al., 2005; Zuo et al., 2005). The labeling of individual neurons by in utero electroporation also allowed for visualization of neuronal morphology including patterns of dendritic arborization. Consistent with our histological findings (Fig. 1, J–N), we could detect no abnormalities in the morphology or dendritic arborization of DLK^{lox};Cre^{pos} neurons (Fig. 3 G). Together, these data indicate that DLK functions at the synapse in the adult brain but the modest changes in basal synaptic strength induced by *DLK* deletion are not sufficient to result in any structural alterations during the time course analyzed.

DLK is required for excitotoxicity-induced JNK activation and neuronal degeneration

Previous studies have demonstrated that DLK is required for stress-induced JNK signaling in DRG neurons after trophic factor deprivation or axonal injury (Ghosh et al., 2011; Watkins et al., 2013), so we next asked whether excitotoxicity-induced JNK activation is also DLK dependent. To test this, we added NMDA to mature hippocampal cultures and assessed levels of DLK/JNK signaling. Robust and reproducible induction of stress-induced JNK activity was observed as early as 30 min after application of 100 μM NMDA, as measured by phosphorylation of the stress-specific JNK target c-Jun (Fig. 4, A and B). Levels of p-JNK were only slightly elevated after NMDA administration, likely as a result of the high levels of physiological JNK1 activity present in neurons that are independent of the JNK2/3-dependent stress response (Coffey et al., 2002). DLK protein levels were also increased, as has been observed

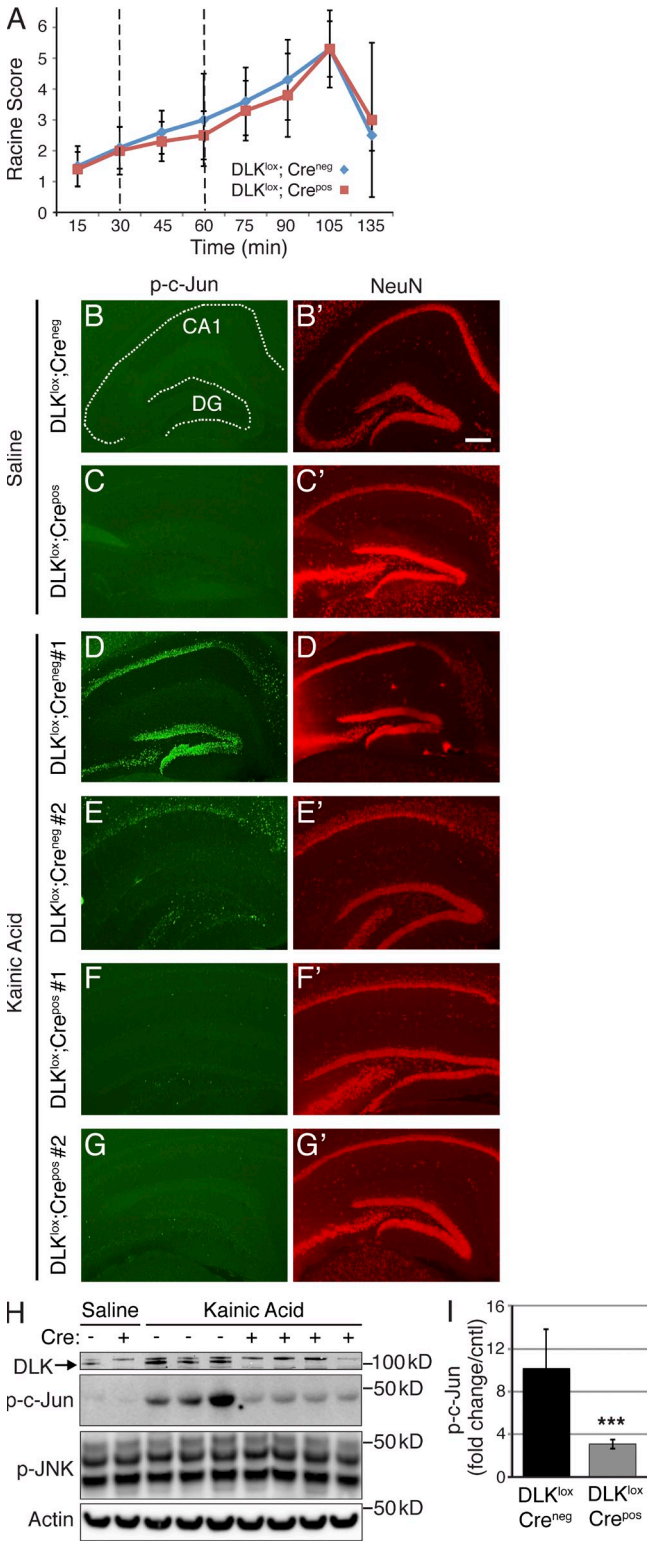

Figure 5. Induction of the JNK-mediated neuronal stress response after kainic acid–induced seizures is attenuated in DLK-inducible knockout mice. (A) Seizure scores for kainic acid–treated DLK^{lox};Cre^{neg} or DLK^{lox};Cre^{pos} mice. Mice were given three i.p. kainic acid injections: one at onset of the experiment and two more at 30-min intervals, as marked by dotted lines. Seizures were qualified according to Racine's scale (0 = nothing, 1 = freezing, 2 = clonic posture, 3 = rearing, 4 = rearing and falling, 5 = continuous rearing and falling, 6 = grand mal seizure, and 7 = death). Values represent the maximum seizure activity during each 15-min increment. n = 10 animals for DLK^{lox};Cre^{neg} and 11 for DLK^{lox};Cre^{pos}. Error bars represent SD. (B–G′) Immunohistochemistry for p-c-Jun and NeuN in the hippocampus of DLK^{lox};Cre^{neg} and DLK^{lox};Cre^{pos} mice 4 h after kainic acid treatment. (B′–G′) p-c-Jun is labeled in green (left), whereas NeuN of the same sections is shown in red (right) to visualize the neuronal architecture of the hippocampus (CA1 = Cornu Ammonis area 1; DG = dentate gyrus). Data are representative of $n \geq 8$ animals/genotype from three independent experiments. Bar, 300 µm. (H) Western blots of hippocampal lysates from kainic acid–treated DLK^{lox};Cre^{neg} or DLK^{lox};Cre^{pos} mice. Cre genotype is annotated by a + or − symbol, and Actin is shown as a protein loading control. Data are representative of three independent experiments. (I) Quantification of p-c-Jun levels in kainic acid–treated DLK^{lox};Cre^{pos} or DLK^{lox};Cre^{neg} mice assessed by Western blot as shown in H. DLK^{lox};Cre^{neg} = 10.2 ± 3.7- and DLK^{lox};Cre^{pos} = 3.12 ± 0.4-fold increase in p-c-Jun compared with controls (n = 10 for DLK^{lox};Cre^{neg} and 11 for DLK^{lox};Cre^{pos}). ***, P < 0.001, unpaired Student's t test; error bars represent SEM.

after axonal injury (Xiong et al., 2010; Huntwork-Rodriguez et al., 2013), implying that DLK may contribute to JNK activation after NMDA application. To examine the functional relevance of DLK in this setting, the induction of JNK and c-Jun phosphorylation after NMDA application were measured in neurons from DLK knockout mice. Interestingly, the NMDA-induced increase in p-c-Jun was significantly attenuated in neurons lacking DLK (Fig. 4, C and D). DLK-null neurons also lacked any increase in p-JNK after NMDA application, arguing that DLK is required for NMDA receptor-induced JNK activation and c-Jun phosphorylation.

The pathways that regulate neuronal excitotoxicity in vitro have been shown to be highly dependent on the protocol and cell type used (Ankarcrona et al., 1995; Bonfoco et al., 1995; Dawson et al., 1996; Mandir et al., 2000), so we chose to assess the role of DLK in this process in vivo using the kainic acid model. This model is characterized by massive glutamate release, seizures, and rapid c-Jun phosphorylation and subsequent NMDA receptor dependent neurodegeneration of hippocampal neurons over a period of days (Ben-Ari, 1985; Yang et al., 1997). 1 wk after completion of the Tamoxifen dosing regimen to excise *DLK*, DLK^{lox};Cre^{pos} and DLK^{lox};Cre^{neg} control mice were injected with kainic acid to induce seizures. Three intraperitoneal injections of 10 mg/kg kainic acid were administered at 30-min intervals (Hellier and Dudek, 2005) to generate more consistent seizures and avoid the high rates of mortality often observed with large bolus injections (McLin and Steward, 2006). This multiple injection protocol triggered severe seizures with maximal seizure scores of 4–6 in both DLK^{lox};Cre^{pos} and DLK^{lox};Cre^{neg} control groups (Fig. 5 A). In DLK^{lox};Cre^{neg} mice, kainic acid injection resulted in robust c-Jun phosphorylation in hippocampal neurons 4 h after the first injection with some variability between animals (Fig. 5, B–G′). In contrast, only a very few scattered p-c-Jun–positive cells were observed in DLK^{lox};Cre^{pos} hippocampi at the same time point. To confirm the reduction in p-c-Jun levels, we analyzed DLK^{lox};Cre^{pos} and control mice 4 h after kainic acid

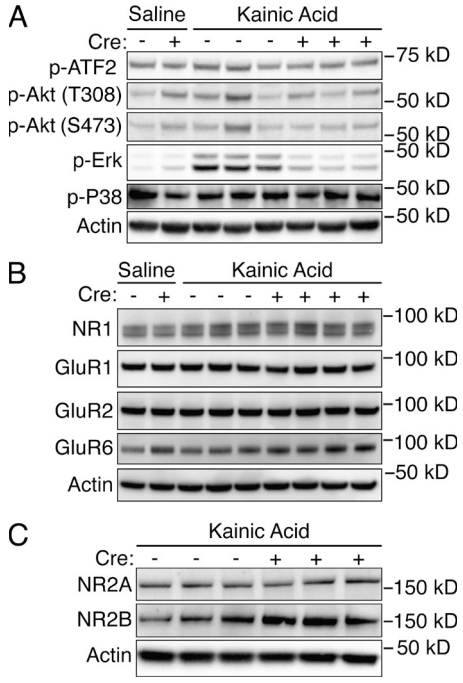

Figure 6. Analysis of additional markers in brains of DLK-inducible knockout mice. (A) Western blots for p-ATF2, p-AKT, p-ERK, and p-P38 in hippocampal lysates from DLK^{lox};Cre^{neg} or DLK^{lox};Cre^{pos} mice treated with saline or kainic acid. Cre genotype is annotated by a + or − symbol, and Actin is shown as a loading control. Data are representative of $n \geq 6$ animals/genotype from two independent experiments. (B) Western blot for NMDA receptor subunit NR1 and various glutamate receptor subunits (GluR1, GluR2, and GluR6) from DLK^{lox};Cre^{neg} and DLK^{lox};Cre^{pos} hippocampi. Cre genotype is annotated by a + or − symbol, and Actin is shown as a protein loading control. Data are representative of $n \geq 6$ animals/genotype from two independent experiments. (C) Western blot for NMDA receptor subunits NR2A and NR2B in hippocampal lysates of kainic acid–treated DLK^{lox};Cre^{neg} and DLK^{lox};Cre^{pos} hippocampi. Cre genotype is annotated by a + or − symbol, and Actin is shown as a protein loading control. A 1.3-fold increase in NR2B was observed in DLK^{lox};Cre^{pos} but this change was not statistically significant ($P = 0.411$, paired Student's *t* test). Data are representative of $n = 6$ animals/genotype from two independent experiments.

administration by Western blotting. Consistent with the immunohistochemical staining, the kainic acid–induced phosphorylation of c-Jun was increased 10.2-fold in hippocampi of DLK^{lox};Cre^{neg} mice, and this induction was largely attenuated in DLK^{lox};Cre^{pos} animals (Fig. 5, H and I). Levels of p-JNK were not found to be elevated after kainic acid administration in either genotype, consistent with our observations in vitro. This suggests that DLK specifically regulates stress-induced JNK activity in the adult brain after insult without affecting other aspects of JNK signaling, as was observed in cultured DRG neurons (Ghosh et al., 2011).

To investigate whether *DLK* deletion modified the activation state of other intracellular signaling pathways in addition to JNK/c-Jun, we examined hippocampal lysates from Tamoxifen-treated DLK^{lox};Cre^{pos} and DLK^{lox};Cre^{neg} 4 h after kainic acid administration. The levels and phosphorylation state of several proteins, including ATF2, Akt, ERK, p38, CDK5, Creb, and c-Fos, were examined based on their known involvement in the neuronal stress response and/or previous studies reporting kainic acid–dependent changes in their activation state. Of all the pathways investigated, only the increased ERK phosphorylation proved to be DLK dependent while others were unaffected by DLK genotype (Fig. 6 A and not depicted). These findings suggest that seizure-induced phosphorylation of ERK is also downstream of DLK signaling, although the mechanism of this regulation may be indirect.

To exclude the possibility that the reduction in p-c-Jun and other alterations observed in DLK^{lox};Cre^{pos} animals was a result of changes in glutamate receptor expression, the levels of various receptors were examined by Western blotting. The NMDA receptor subunit NR1, GluR1, GluR2, and GluR6 appeared equivalent in all samples regardless of genotype (Fig. 6 B). Analysis of other NMDA receptor subunits detected a 1.3-fold increase in NR2B levels in DLK^{lox};Cre^{pos} animals as compared with DLK^{lox};Cre^{neg} littermates (Fig. 6 C), which would not likely be sufficient to have any functional effects (Papouin et al., 2012). Therefore, the differences in phospho-c-Jun levels observed in DLK-inducible knockout mice arise from inhibition of the signaling cascade downstream of the NMDA receptor rather than alterations in the expression of particular glutamate receptor components.

Loss of DLK protects neurons against excitotoxicity-induced degeneration

To determine if the loss of DLK expression would be sufficient to protect neurons from degeneration, we measured various markers of neuronal cell death in hippocampi of Tamoxifen-treated DLK^{lox};Cre^{neg} mice and DLK^{lox};Cre^{pos} littermates 7 d after kainic acid administration. First, neuronal apoptosis was examined using TUNEL staining. Although no TUNEL-positive cells were detected in saline-treated control animals of either genotype (not depicted), a considerable number of TUNEL-positive neurons were observed in the CA1 and CA3 regions of the hippocampus in DLK^{lox};Cre^{neg} animals along with scattered cells in the dentate gyrus and cortex (Fig. 7 A). In DLK^{lox};Cre^{pos} mice, however, the number of TUNEL-positive cells in all regions was significantly reduced and nearly absent in most mice (Fig. 7 B). Quantification of TUNEL-positive cells in the CA1 region of each animal revealed an ∼24-fold decrease DLK^{lox};Cre^{pos} as compared with DLK^{lox};Cre^{neg} mice at this time point (Fig. 7 C). To confirm that neurons in DLK^{lox};Cre^{pos} were not lost via necrosis or other caspase-independent degeneration pathways that would not be detected by TUNEL labeling, we stained a subset of hippocampal sections from kainic acid–treated DLK^{lox};Cre^{neg} and DLK^{lox};Cre^{pos} animals with NeuN and measured the number of remaining CA1 neurons as compared with saline-treated controls. Notably, in DLK^{lox};Cre^{neg} mice which displayed increased TUNEL reactivity, we observed a thinning of the CA1 region, whereas significant levels of neuronal loss were not seen in DLK^{lox};Cre^{pos} animals (Fig. 7, D-E′). Quantification of the mean NeuN-positive neurons per section revealed

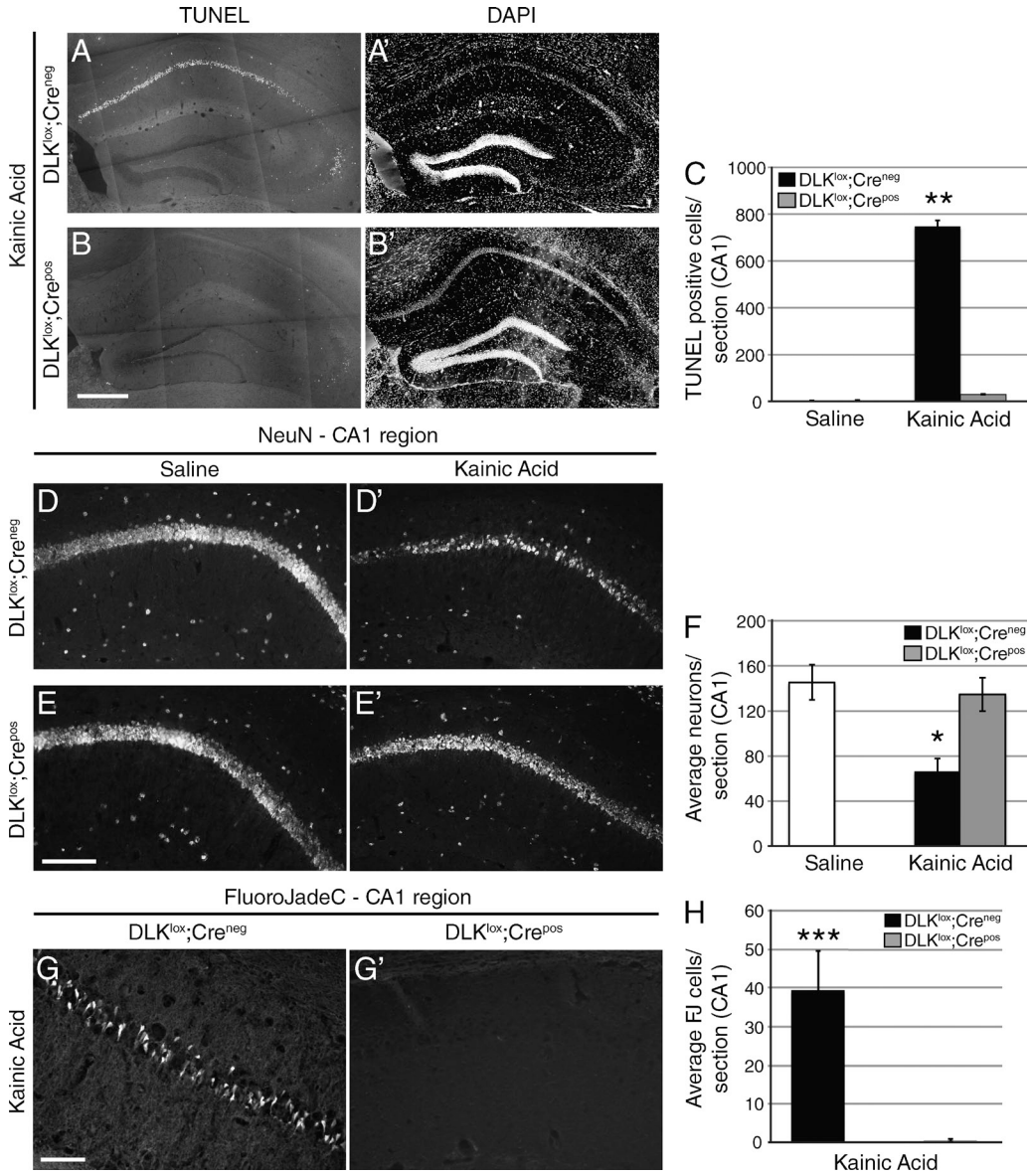

Figure 7. DLK-inducible knockout mice are protected from kainic acid–induced neuronal degeneration. (A–B′) Images of TUNEL and DAPI staining in the hippocampus of $DLK^{lox};Cre^{neg}$ and $DLK^{lox};Cre^{pos}$ mice 7 d after treatment with kainic acid. TUNEL is shown on the left (A and B), and DAPI staining of the same sections on the right (A′ and B′) to visualize the neuronal architecture of the hippocampus. Bar, 300 µm. (C) Quantification of TUNEL labeling shown in A–B′. The graph represents the mean number of TUNEL-positive cells quantified per section of the CA1 region. (Saline: $DLK^{lox};Cre^{neg}$ = 7.2 ± 1.1, n = 2; $DLK^{lox};Cre^{pos}$ = 4.9 ± 0.8, n = 2; kainic acid: $DLK^{lox};Cre^{neg}$ = 748 ± 84.5, n = 11; $DLK^{lox};Cre^{pos}$ =31 ± 4.27, n = 11; **, $P < 0.01$. Error bars represent SEM.) (D–E′) NeuN immunohistochemistry in the CA1 region of hippocampus in saline- or kainic acid–treated mice. D and D′ depict $DLK^{lox};Cre^{neg}$ animals and E and E′ show $DLK^{lox};Cre^{pos}$ animals. Bar, 100 µm. (F) Quantification of NeuN labeling shown in D–E′. The graph represents the mean number of NeuN-positive neurons per section in the CA1 region (saline = 146 ± 16, n = 2/genotype; kainic acid: $DLK^{lox};Cre^{neg}$ = 67 ± 12 n = 5; $DLK^{lox};Cre^{pos}$=135 ± 15, n = 5; *, $P < 0.05$, Student's t test. Error bars represent SEM. (G and G′) Fluoro-Jade C staining in the CA1 region of the hippocampus in kainic acid–treated $DLK^{lox};Cre^{neg}$ (G) and $DLK^{lox};Cre^{pos}$ (G′) mice. Bar, 50 µm. (H) Quantification of Fluoro-Jade C staining shown in G and G′. ($DLK^{lox};Cre^{neg}$ = 39.6 ± 10.6, n = 11; $DLK^{lox};Cre^{pos}$ = 0.48 ± 1.4, n = 11; ***, $P < 0.001$, paired Student's t test. Error bars represent SEM).

an approximately twofold decrease in the number of neurons in $DLK^{lox};Cre^{neg}$ animals as compared with $DLK^{lox};Cre^{pos}$ ($P < 0.05$; Fig. 7 F), indicating that both apoptotic and nonapoptotic mechanisms of cell death are reduced in $DLK^{lox};Cre^{pos}$ animals treated with kainic acid.

To examine whether neurons in $DLK^{lox};Cre^{pos}$ mice displayed any sign of overt neuronal degeneration that was insufficient to induce cell death, we stained brain sections from $DLK^{lox};Cre^{neg}$ and $DLK^{lox};Cre^{pos}$ with Fluoro-Jade C, a marker which labels degenerating neurons including affected neuronal processes (Schmued et al., 1997). Significant Fluoro-Jade C staining was observed in CA1 regions of $DLK^{lox};Cre^{neg}$ mice, but little to no staining was evident in the hippocampus of $DLK^{lox};Cre^{pos}$ animals (Fig. 7, G and G′). Quantification

revealed a decrease (~80-fold) in total levels of Fluoro-Jade C staining in DLK^{lox};Cre^{pos} mice after kainic acid treatment (Fig. 7 H). Collectively, these results indicate that loss of DLK results in a significant decrease in the levels of neuronal degeneration that result from kainic acid injection during the time points analyzed.

DISCUSSION

In this study, we demonstrate that DLK is present at the postsynaptic density and is an essential regulator of neuronal degeneration after excitotoxic injury in the adult central nervous system. This represents a departure from previous studies that have demonstrated neuroprotective phenotypes resulting from DLK deletion, all of which are dependent on insults that originate in the axon (Chen et al., 2008; Miller et al., 2009; Ghosh et al., 2011; Shin et al., 2012). The divergent DLK localization and function described here argues that DLK may regulate neuronal degeneration in contexts such as cerebral ischemia, where excitotoxicity is a predominant driver of neuronal cell death. In addition, the diversity of degenerative phenotypes now shown to be DLK-dependent implies that it may act more broadly as a regulator of neuronal degeneration in development and disease.

The neuroprotective effects elicited by DLK removal suggest that DLK would be an attractive therapeutic target for treatment of stroke and related neurodegenerative indications; several key observations made in this study lend support to this conclusion. First, DLK deletion appears to protect neurons from both the apoptotic and nonapoptotic cell death that are thought to occur after kainic acid administration (Ferrer et al., 1995). A similar mixture of degeneration is known to occur after ischemic insult (Charriaut-Marlangue et al., 1996; Snider et al., 1999) and our data implies that DLK/JNK may be involved in initiation of cell death via either mechanism. Second, loss of DLK alone was sufficient to generate a significant reduction in the phosphorylation of the stress-specific JNK target c-Jun downstream of glutamate receptor hyperactivation without affecting overall JNK activity (Fig. 4, C and D). The JNK genes, particularly JNK3, have long been pursued as targets for the treatment of cerebral ischemia based on the observation that inhibition of signaling similarly reduces excitotoxicity-driven neuronal degeneration (Yang et al., 1997; Borsello et al., 2003; Kuan et al., 2003). However, JNK1 has been shown to have important non–stress-related functions in neurons (Chang et al., 2003; Tararuk et al., 2006), and obtaining specific, brain-penetrant inhibitors of JNK3 has proven extremely difficult (Waetzig and Herdegen, 2005; Bogoyevitch et al., 2010). Targeting DLK may provide an alternative approach to more specifically target JNK pathway-dependent neuronal degeneration. Third, although the data presented here demonstrates that DLK is essential for neuronal degeneration downstream of NMDA receptor hyper-activation (Fig. 6, B and C), the normal viability of Tamoxifen-treated DLK^{lox};Cre^{pos} animals suggests that inhibition of DLK would not be expected to demonstrate the same type of toxicity that plagued NMDA receptor antagonists (Muir, 2006). However, a complete behavioral and electrophysiological assessment of DLK^{lox};Cre^{pos} mice will be required to definitively address the consequences of DLK deletion/inhibition in unstressed neurons.

The DLK-interacting partners identified in this study are consistent with DLK acting, at least in part, at the synapse to direct JNK activation and neuronal degeneration after NMDA receptor hyper-activation. Specifically, the interaction of DLK with PSD-95, a core component of postsynaptic machinery which is essential for proper synaptic function (Migaud et al., 1998), argues that DLK protein is specifically targeted to the synapse rather than being present through passive diffusion. This hypothesis is further substantiated by the interaction identified between DLK and other PSD proteins, such as Syngap1, a PSD-95–interacting protein which regulates MAPK activity (Kim et al., 1998). This postsynaptic localization of DLK provides an appealing explanation for how excitotoxic stress is coupled to JNK activation, as JNKs have not been identified as present at the synapse (Collins et al., 2006). Interestingly, the previously identified DLK interactor JIP3 (Ghosh et al., 2011) was not identified in our screen and may reflect the differences between DLK function in the adult versus the embryo. Alternatively, given the interconnected network of protein–protein interactions at the PSD (Sheng and Kim, 2011), it is possible that minor differences in the protocols used to enrich DLK-interacting proteins could alter the composition and relative stoichiometry of proteins captured. Consistent with this hypothesis, a recent mass spectrometry–based study examining JIP3-interacting proteins identified >100 direct and indirect interactors but no MAP kinases (Abe et al., 2009), despite several studies confirming that these proteins indeed interact (Kelkar et al., 2000; Cavalli et al., 2005; Ghosh et al., 2011). Likewise, the stringent post-acquisition filtering criteria used in our study likely resulted in the exclusion of a subset of bona fide DLK-interacting proteins.

Interestingly, we did not observe a reduction in seizure intensity in DLK^{lox};Cre^{pos} mice after kainic acid administration, as was previously described in JNK3 knockouts or animals expressing a mutant c-Jun that cannot be phosphorylated (Behrens et al., 1999; Yang et al., 1997). This discrepancy could be explained by the different protocols used in each study, as the multiple kainic acid injections used here may have overcome a suppressed seizure response. Alternatively, this discrepancy may be a result of the strengthening in synaptic signaling observed in DLK^{lox};Cre^{pos} mice (Fig. 3 A). In either case, the normal neuronal morphology and viability in Tamoxifen-treated DLK^{lox};Cre^{pos} mice suggests that DLK may function predominantly as a stress sensor in the adult brain, similar to what has previously been described in axonal injury paradigms. It is possible that DLK also induces neuronal degeneration in chronic paradigms such as Alzheimer's disease, Parkinson's disease, or even environmental stresses. Indeed, there is precedence for JNK pathway activation and function in each of these instances (Saporito et al., 1999; Morishima et al., 2001; Hunot et al., 2004; Thakur et al., 2007; Sherrin et al., 2010), all of which have the potential to be DLK dependent.

In conclusion, the results described here define a function for DLK in the adult brain that mirrors previously described roles during development and point to the DLK/JNK pathway as a conserved mechanism that directs neuronal degeneration in response to a variety of insults.

MATERIALS AND METHODS

Generation of mice. DLK-inducible knockout mice were generated using the same construct and ES cells previously described (Ghosh et al., 2011). CAG-Cre-ERT mice (The Jackson Laboratory) have been previously described (Hayashi and McMahon, 2002). To induce *DLK* recombination mice were fed Tamoxifen chow for 21 d (animals ingest roughly 40 mg/kg/d) and on day 22, mice were taken off Tamoxifen diet and put back on regular chow for an additional week. For the kainic acid experiments, mice were also dosed i.p. with 200 mg/kg Tamoxifen in corn oil on days 8, 10, and 12. For experiments aimed to assess the long-term effects of DLK knockdown in the adult brain and the microarray experiment, mice were fed Tamoxifen chow for 21 d and then switched back to regular food for an additional 12 or 9 wk, respectively. *DLK* was assessed in various brain and tail samples using PCR methods previously described (Ghosh et al., 2011), and all protocols resulted in a sufficient reduction in DLK levels. DLK knockout mice used in some of the in vitro experiments were generated as previously described (Ghosh et al., 2011).

Western blotting and immunoprecipitation. Tissues were lysed in ice-cold RIPA buffer (150 mM NaCl, 50 mM Tris, pH 8.0, 1% NP-40, and protease and phosphatase inhibitors) using the TissueLyzer (frequency 30/s, 6 min at 4°C; QIAGEN). Fractions from adult rat brain were isolated as previously described (Zhu et al., 2005). According to this method, P2 contains crude synaptosomes, PSDI Triton X-100 insoluble synaptosomes, and PSDII insoluble core PSD proteins. For mouse cortical (E15–16) or rat hippocampal (E17–18) neurons, media was removed, cells were rinsed with cold PBS, and RIPA buffer was added directly to the plate to lyse the cells and neurons collected using a cell scraper (Falcon). Lysates were rocked for 30 min at 4°C and then centrifuged (14,000 rpm, 4°C) for 30 min. Protein amounts were quantified using bicinchoninic acid (BCA) protein assay reagent (Thermo Fisher Scientific). Samples were resuspended in 4× NuPAGE sample buffer (Invitrogen), boiled for 5 min, subjected to SDS/PAGE (4–12% gradient Bis-Tris; Invitrogen), and transferred to a nitrocellulose membrane (Invitrogen). Membranes were blocked for 30–60 min in 5% nonfat milk in Tris-buffered saline + Tween 20 (TBST) at room temperature and then incubated overnight in primary antibody at 4°C. Membranes were washed three times in TBST (10 mM TRIS, pH 8.0, 150 mM NaCl, and 0.1% Tween 20), incubated in HRP-conjugated secondary antibody (1:5,000) for 2 h, and then washed again 3× in TBST. Proteins were detected with Westdura HRP substrate (Thermo Fisher Scientific) and visualized on Versadoc or Chemidoc imager (Bio-Rad Laboratories). Densitometry was performed with Image Lab software (Bio-Rad Laboratories) and statistical significance determined by two-way ANOVA or Student's *t* test. Primary antibodies used were as follows: DLK, 1:1,000 (Genentech); PSD-95 K28 clone, 1:500 (Millipore); PSD-95, 1:500 (Abcam); Tubulin, 1:1,000 (Covance); NR1, 1:1,000 (Abcam); NR2A, 1:1,000 (Phosphosolutions); NR2B, 1:500 (Abcam or Covance); GluR1, 1:1,000 (Millipore); GluR2, 1:1,000 (Millipore); GluR6, 1:1,000 (Millipore); H2B, 1:1,000 (Millipore); p-c-Jun, 1:500 (Cell Signaling Technology); p-JNK, 1:1,000 (Cell Signaling Technology); GSK3β, 1:1,000 (Cell Signaling Technology); GAPDH, 1:2,000 (Cell Signaling Technology); rabbit IgG (Sigma-Aldrich); phospho-ATF2, 1:1,000; phospho Akt (Thr 308 and Ser473), 1:1,000; phospho ERK, 1:1,000; phospho p38, 1:1,000 (Cell Signaling Technology); and actin, 1:2,000 (Sigma-Aldrich). Immunoblots were quantified by Image-Lab software (Bio-Rad Laboratories).

For immunoprecipitation experiments, adult mouse brains were homogenized in Triton X-100 lysis buffer (20 mM Tris, pH 7.5, 150 mM NaCl, and 0.1% Triton X-100 with protease and phosphatase inhibitors). Protein amounts were quantified with BCA and 0.5–1.0 mg of protein was used for each immunoprecipitation, along with Protein A– Sepharose beads (GE Healthcare) and antibodies to DLK, PSD-95 (Abcam), or a nonspecific rabbit IgG antibody (Sigma-Aldrich). Beads were washed 5× in lysis buffer and proteins were eluted off the beads by boiling in 2× sample buffer. 10% of protein was run as input while ∼80% of the pulldown was run in each lane. The experiment was repeated at least 3× on both mouse and rat brain with similar results.

Mass spectrometry and data analysis. Immunoprecipitations were resolved by SDS-PAGE and stained with Simply Blue Safe Stain (Invitrogen). Each lane was cut into 14 regions to be reduced, alkylated, and digested overnight with trypsin (Promega). Extracted peptides were analyzed on an LTQ Orbitrap (Thermo Fisher Scientific) using a top 8 method over a 60-min gradient. Data were searched against concatenated human and mouse entries in UniProt using Mascot (Matrix Science) with the following parameters: precursor tolerance 50 ppm, MS/MS 0.8 D, ≤2 missed cleavages, oxidized methionine and carbamidomethylated cysteine as variable modifications. Spectral match data were filtered to 1% false discovery rate using linear discriminant analysis.

Microarray analysis. RNA was extracted from DLK^{lox};Cre^{neg} and DLK^{lox};Cre^{pos} hippocampi (QIAGEN) and microarrays were performed as previously described (Watkins et al., 2013). The data were analyzed using the open source statistical software R (v 3.0) and Bioconductor (v 2.12). Raw expression data were background corrected and normalized with the loess method with the normalize Within Arrays and normalize Between Arrays functions in the limma package. Expression probes were filtered with the featureFilter function in genefilter so that a single probe represented the expression of each gene. Differential expression for each gene, *i*, was determined by fitting the following linear model in the limma package: $Expression = \beta_{0i} + \beta_{1i} * Genotype$. P-values of the moderated T-statistic were adjusted for multiple testing with the Benjamini and Hochberg method. Complete microarray data can be found under GEO accession no. GSE50245.

Electrophysiology. 400–500-µm horizontal slices containing hippocampus were prepared with a vibrating sectioning system (Leica) and were recorded in oxygenated Artificial Cerebrospinal Fluid (ACSF) containing (in millimoles) 127 NaCl, 2.5 KCl, 1.3 $MgSO_4$, 2.5 $CaCl_2$, 1.25 Na_2HPO_4, 25 $NaHCO_3$ and 25 mM glucose. Slices were prepared in ice-cold oxygenated ACSF with the $MgSO_4$ concentration elevated to 7 mM, NaCl replaced with 110 mM choline and with 11.6 mM Na-ascorbate, and 3.1 mM Na-pyruvate. Field recordings of EPSPs were measured from the stratum radiatum of CA1 in response to stimulation of Schaffer collateral inputs. PPRs were measured by dividing the slope of the second EPSP by the slope of the first EPSP evoked using paired stimulations. Significance was assessed by comparing the PPRs of each genotype using a Student's *t* test. Input-output relationships were measured by stimulating at 15 logarithmically spaced stimulus intensities ranging from 40 to 240 mA. Significance was assed using a two-way ANOVA with genotype and stimulus intensity as the factors. LTP was induced using one, two, or three bouts of theta burst stimulation separated by 20 s, each consisting of five pulses at 100 Hz repeated 10 times at 200-ms intervals. Significance was assessed by comparing the mean EPSP slope at the last 10 min of recording post-LTP induction in each genotype using a Student's *t* test.

In utero electroporation and spine density analysis. Progenitor cells of cortical layer II/III excitatory neuron were electroporated at E16.5, as described previously (Saito and Nakatsuji, 2001). DLK^{lox};Cre^{neg} embryos were injected with plasmid cocktails containing, as indicated in the text, pCAGGS-based plasmids containing the cDNA for DsRed-Express (Takara Bio Inc.), Cre, or EGFP flanked by lox sites (Atasoy et al., 2008). Cortical neural precursors in DLK^{lox};Cre^{neg} day 16.5 embryos were electroporated with DsRed-Express to label electroporated neurons, a Cre expression construct, and Cre recombinase–sensitive GFP to confirm *DLK* recombination in electroporated neurons (referred to as Cre^{+}), whereas control animals received DsRed-Express and Cre recombinase-sensitive GFP plasmids only (Cre^{-}). This strategy ensures that GFP-labeled neurons are expressing Cre and that any

observed DLK-dependent alteration in neuronal morphology is cell autonomous. At postnatal day 30, animals were perfused with 4% PFA in PBS, brains harvested, incubated overnight in 4% PFA, and then washed in PBS. Apical dendrites and their spines were imaged en bloc via two-photon microscopy (Prairie Technologies) using a 40× objective (Olympus) with pixel resolution of 0.0852 µm/pixel across a 1,024 × 1,024 field of view. Dendritic spine density and size measures were generated using custom image analysis routines in MatLab (Mathworks). Spine density was estimated as the total number of visible dendritic spines divided by the corresponding length of dendrite. Relative spine volumes were estimated for each detected spine based on the number of corresponding DsRed-Express+ pixels in xyz dimensions above a local threshold applied as part of an automated image segmentation algorithm. Low magnification images of cortical neurons were acquired using a 20× objective (Olympus) with pixel resolution of 0.2092 µm/pixel across a 1,024 × 1,024 field of view.

Immunocytochemistry and imaging. Cultured neurons were fixed with 4% PFA/4% sucrose/PBS for 15 min at room temperature, washed three times with PBS, and then blocked in PBS+0.1% Triton X-100 for 30 min. Neurons were incubated with primary antibodies overnight at 4°C (anti-Map2, 1:2,000; Abcam; anti–PSD-95 (K28), 1:500, Millipore; anti-DLK, 1:500, Genentech) and then washed 3× with PBS. Neurons were incubated with secondary antibodies (Alexa Fluor 488/568/633, 1:400; Invitrogen) for 2 h at room temperature, washed 3× with PBS and mounted in Fluoromount-G (Vector Laboratories). Neurons were imaged on a confocal microscope (LSM710; Carl Zeiss) using a 40 or 100× objective as a flattened z-stack and presented as maximum intensity projections. Brightness and contrast were altered to more easily visualize the signal in Fig. 2 using Photoshop (Adobe), but all data within a panel were identically imaged and modified. Quantification of the PSD-95 and DLK colocalization was obtained in a blinded fashion by analyzing three dimensional reconstruction of Z-stack images using Volocity software as previously described (Ayalon et al., 2008).

Primary neuron cultures and NMDA treatment. E17-E18 rat hippocampi or E15–16 mouse cortical neurons were dissected and digested with 0.05% Trypsin (Worthington) for 20 min at 37°C. DNase (Sigma-Aldrich) was added for 3 min at room temperature and a single cell suspension was generated by gentle trituration using a P1000 pipetman (Rainin). The cortical cell suspension was layered on top of cushion of heat inactivated fetal bovine serum (1:1, FBS; Invitrogen) and spun in a tabletop centrifuge (CentraCL2; Thermo Fisher Scientific) at 1,000 rpm for 5 min to remove glial cells. The cell pellet was gently resuspended in 1ml of NbActive4 media (BrainBits) + 1% penstrep (Invitrogen) and cells were counted using a cell counter (Immunicon) before being plated on precoated poly-D-lysine chamber slides, 12- or 6-well dishes (Biocoat; BD) at densities of 25,000, 240,000, or 0.5×10^6 cells per well, respectively, and incubated at 37°C, 5% CO_2. Every third day, half of the media was removed and replaced with fresh NbActive4.

For NMDA experiments, conditioned media was removed and collected from 21–28 DIV rat hippocampal neurons or 14 DIV mouse cortical neurons. Cultures were over laid with sterile artificial CSF (aCSF; 119 mM NaCl, 26.2 mM $NaHCO_3$, 2.5 mM KCl, 1 mM NaH_2PO_4, 1.3 mM $MgCl_2$, 10 mM glucose, 2 mM $CaCl_2$, 20 µM glycine) and treated with 100 µM NMDA for 30 min at 37°C. NMDA containing aCSF was removed and conditioned media mixed with fresh NbActive4 (1:1 ratio) was added back to cultures which were incubated for an additional 30, 60, 90, 120, or 240 min before lysis.

Kainic acid treatment and tissue processing. All experiments with mice were performed under animal protocols approved by the Animal care and Use Committee at Genentech Inc. Kainic acid powder (Tocris) was reconstituted in 22 mM NaOH, 0.9% sterile saline (Sigma-Aldrich), and kept on ice throughout the experiment. DLK^{lox};Cre^{neg} and DLK^{lox};Cre^{pos} mice that had been treated previously with Tamoxifen were injected i.p. with 10-25 mg/kg fresh Kainic acid at time 0, 30, and 60 min. Animals were observed and behavior was scored every 5 min according to Racine's scale. Control animals were injected with sterile saline. Animals were deeply anesthetized using i.p. injection of 0.5 mg/g Avertin 4 h or 7 d after treatment and then transcardially perfused with cold PBS, pH 7.4, followed by 4% paraformaldehyde. The brains were dissected, postfixed overnight at 4°C, and then cryoprotected in 30% sucrose/PBS. Frozen brains were sectioned on a cryostat at 20 µM and every third sample collected and mounted on a gelatin coated glass slide (LabScientific).

Immunohistochemistry, TUNEL, and Fluoro-Jade C staining. Mouse brain tissue was washed in PBS for 5 min then blocked in 5% normal goat serum (Vector Laboratories) in PBS+0.5% Triton X-100 (PBST) for 30–60 min at room temperature. Sections were incubated with NeuN (mouse, 1:500; Millipore) for 2 h at room temperature or overnight at 4°C. After incubation, sections were washed three times in PBS, incubated with secondary antibodies (Alexa Fluor 488 and 546; Molecular Probes) for 2 h in the dark at room temperature, washed again 3× in PBS, and mounted in Fluoromount-G (Vector Laboratories). Fluoro-Jade C staining was done on frozen sections according to the manufacturer's protocol (Millipore). Brightness and contrast were altered to more easily visualize the signal in Figs. 5 and 7 using Photoshop (Adobe), but all data within a panel were identically imaged and modified.

Fluorescent images were acquired using a microscope (DM5500; Leica) with a camera (DFC360) and a 5, 10, or 20× objective and imaging software (Leica). Chromogenic immunohistochemistry and Nissl staining was done according to proprietary methods at Neuroscience Associates (Knoxville, TN). Bright field images were acquired using a 20 or 40× objective and Leica imaging software. Equivalent regions of interest within the CA1 were compared between saline or kainic acid–treated animals of each genotype. The numbers of NeuN-positive CA1 pyramidal neurons were manually counted in two sections per animal and mean number of NeuN-positive cells per section was graphed. Identical methods were used to quantify Fluoro-Jade C–positive cells in the kainic acid–treated DLK^{lox};Cre^{neg} and DLK^{lox};Cre^{pos} CA1 region and mean number per section per genotype was graphed. Differences between DLK^{lox};Cre^{neg} and DLK^{lox};Cre^{pos} animals were analyzed with unpaired (NeuN) and paired (FluoroJade-C) Student's *t* tests.

For TUNEL labeling, mouse brain tissue was washed in PBS for 5 min and then permeabilized with an ice-cold methanol/ethanol solution (2:1) at −20°C for 5 min. Slides were washed in PBS and labeled with the Live/Dead Fluorescein TUNEL kit (Promega) according to the manufacturer's protocol. The same sections were co-stained with antibodies to NeuN as described above. Quantification of TUNEL-positive cells in the CA1 region was conducted in a blinded fashion using Leica imaging software and manual counting methods, or a journal written to quantify total TUNEL-positive cells per area using MetaMorph software (Molecular Devices). A comparison of both methods yielded nearly identical results. The mean number of TUNEL-positive cells per CA1 area was calculated for each animal and the sums of the means are depicted in the graph. Differences between DLK^{lox};Cre^{neg} and DLK^{lox};Cre^{pos} animals were analyzed with a one-way ANOVA.

We would like to thank William Meilandt for his assistance developing the kainic acid protocol, Dara Kallop for assistance with in utero electroporations, Melissa Gonzalez-Edick for help with slide imaging, Peter S. Liu for assistance with mass spectrometry studies, Zora Modrusan for microarray studies, and Nicholas Lewin-Koh for help with statistical analysis.

All authors are employees of Genentech, Inc.

The authors have no additional financial interests.

Submitted: 21 December 2012
Accepted: 25 September 2013

REFERENCES

Aarts, M., Y. Liu, L. Liu, S. Besshoh, M. Arundine, J.W. Gurd, Y.T. Wang, M.W. Salter, and M. Tymianski. 2002. Treatment of ischemic brain damage by perturbing NMDA receptor- PSD-95 protein interactions. *Science.* 298:846–850. http://dx.doi.org/10.1126/science.1072873

Abe, N., A. Almenar-Queralt, C. Lillo, Z. Shen, J. Lozach, S.P. Briggs, D.S. Williams, L.S. Goldstein, and V. Cavalli. 2009. Sunday driver interacts

with two distinct classes of axonal organelles. *J. Biol. Chem.* 284:34628–34639. http://dx.doi.org/10.1074/jbc.M109.035022

Ankarcrona, M., J.M. Dypbukt, E. Bonfoco, B. Zhivotovsky, S. Orrenius, S.A. Lipton, and P. Nicotera. 1995. Glutamate-induced neuronal death: a succession of necrosis or apoptosis depending on mitochondrial function. *Neuron.* 15:961–973. http://dx.doi.org/10.1016/0896-6273(95)90186-8

Atasoy, D., Y. Aponte, H.H. Su, and S.M. Sternson. 2008. A FLEX switch targets Channelrhodopsin-2 to multiple cell types for imaging and long-range circuit mapping. *J. Neurosci.* 28:7025–7030. http://dx.doi.org/10.1523/JNEUROSCI.1954-08.2008

Ayalon, G., J.Q. Davis, P.B. Scotland, and V. Bennett. 2008. An ankyrin-based mechanism for functional organization of dystrophin and dystroglycan. *Cell.* 135:1189–1200. http://dx.doi.org/10.1016/j.cell.2008.10.018

Behrens, A., M. Sibilia, and E.F. Wagner. 1999. Amino-terminal phosphorylation of c-Jun regulates stress-induced apoptosis and cellular proliferation. *Nat. Genet.* 21:326–329. http://dx.doi.org/10.1038/6854

Ben-Ari, Y. 1985. Limbic seizure and brain damage produced by kainic acid: mechanisms and relevance to human temporal lobe epilepsy. *Neuroscience.* 14:375–403. http://dx.doi.org/10.1016/0306-4522(85)90299-4

Bogoyevitch, M.A., K.R. Ngoei, T.T. Zhao, Y.Y. Yeap, and D.C. Ng. 2010. c-Jun N-terminal kinase (JNK) signaling: recent advances and challenges. *Biochim. Biophys. Acta.* 1804:463–475. http://dx.doi.org/10.1016/j.bbapap.2009.11.002

Bonfoco, E., D. Krainc, M. Ankarcrona, P. Nicotera, and S.A. Lipton. 1995. Apoptosis and necrosis: two distinct events induced, respectively, by mild and intense insults with N-methyl-D-aspartate or nitric oxide/superoxide in cortical cell cultures. *Proc. Natl. Acad. Sci. USA.* 92:7162–7166. http://dx.doi.org/10.1073/pnas.92.16.7162

Borsello, T., P.G. Clarke, L. Hirt, A. Vercelli, M. Repici, D.F. Schorderet, J. Bogousslavsky, and C. Bonny. 2003. A peptide inhibitor of c-Jun N-terminal kinase protects against excitotoxicity and cerebral ischemia. *Nat. Med.* 9:1180–1186. http://dx.doi.org/10.1038/nm911

Cavalli, V., P. Kujala, J. Klumperman, and L.S. Goldstein. 2005. Sunday Driver links axonal transport to damage signaling. *J. Cell Biol.* 168:775–787. http://dx.doi.org/10.1083/jcb.200410136

Chang, L., Y. Jones, M.H. Ellisman, L.S. Goldstein, and M. Karin. 2003. JNK1 is required for maintenance of neuronal microtubules and controls phosphorylation of microtubule-associated proteins. *Dev. Cell.* 4:521–533. http://dx.doi.org/10.1016/S1534-5807(03)00094-7

Charriaut-Marlangue, C., I. Margaill, A. Represa, T. Popovici, M. Plotkine, and Y. Ben-Ari. 1996. Apoptosis and necrosis after reversible focal ischemia: an in situ DNA fragmentation analysis. *J. Cereb. Blood Flow Metab.* 16:186–194. http://dx.doi.org/10.1097/00004647-199603000-00002

Chen, X., M. Rzhetskaya, T. Kareva, R. Bland, M.J. During, A.W. Tank, N. Kholodilov, and R.E. Burke. 2008. Antiapoptotic and trophic effects of dominant-negative forms of dual leucine zipper kinase in dopamine neurons of the substantia nigra in vivo. *J. Neurosci.* 28:672–680. http://dx.doi.org/10.1523/JNEUROSCI.2132-07.2008

Choi, D.W. 1985. Glutamate neurotoxicity in cortical cell culture is calcium dependent. *Neurosci. Lett.* 58:293–297. http://dx.doi.org/10.1016/0304-3940(85)90069-2

Coffey, E.T., G. Smiciene, V. Hongisto, J. Cao, S. Brecht, T. Herdegen, and M.J. Courtney. 2002. c-Jun N-terminal protein kinase (JNK) 2/3 is specifically activated by stress, mediating c-Jun activation, in the presence of constitutive JNK1 activity in cerebellar neurons. *J. Neurosci.* 22:4335–4345.

Collins, M.O., H. Husi, L. Yu, J.M. Brandon, C.N. Anderson, W.P. Blackstock, J.S. Choudhary, and S.G. Grant. 2006. Molecular characterization and comparison of the components and multiprotein complexes in the postsynaptic proteome. *J. Neurochem.* 97:16–23. http://dx.doi.org/10.1111/j.1471-4159.2005.03507.x

Cook, D.J., L. Teves, and M. Tymianski. 2012. Treatment of stroke with a PSD-95 inhibitor in the gyrencephalic primate brain. *Nature.* 483:213–217. http://dx.doi.org/10.1038/nature10841

Dawson, V.L., V.M. Kizushi, P.L. Huang, S.H. Snyder, and T.M. Dawson. 1996. Resistance to neurotoxicity in cortical cultures from neuronal nitric oxide synthase-deficient mice. *J. Neurosci.* 16:2479–2487.

Ferrer, I., F. Martin, T. Serrano, J. Reiriz, E. Pérez-Navarro, J. Alberch, A. Macaya, and A.M. Planas. 1995. Both apoptosis and necrosis occur following intrastriatal administration of excitotoxins. *Acta Neuropathol.* 90:504–510. http://dx.doi.org/10.1007/BF00294812

Gao, Y., A.P. Signore, W. Yin, G. Cao, X.M. Yin, F. Sun, Y. Luo, S.H. Graham, and J. Chen. 2005. Neuroprotection against focal ischemic brain injury by inhibition of c-Jun N-terminal kinase and attenuation of the mitochondrial apoptosis-signaling pathway. *J. Cereb. Blood Flow Metab.* 25:694–712. http://dx.doi.org/10.1038/sj.jcbfm.9600062

Ghosh, A.S., B. Wang, C.D. Pozniak, M. Chen, R.J. Watts, and J.W. Lewcock. 2011. DLK induces developmental neuronal degeneration via selective regulation of proapoptotic JNK activity. *J. Cell Biol.* 194:751–764. http://dx.doi.org/10.1083/jcb.201103153

Hardingham, G.E., and H. Bading. 2010. Synaptic versus extrasynaptic NMDA receptor signalling: implications for neurodegenerative disorders. *Nat. Rev. Neurosci.* 11:682–696. http://dx.doi.org/10.1038/nrn2911

Hayashi, S., and A.P. McMahon. 2002. Efficient recombination in diverse tissues by a tamoxifen-inducible form of Cre: a tool for temporally regulated gene activation/inactivation in the mouse. *Dev. Biol.* 244:305–318. http://dx.doi.org/10.1006/dbio.2002.0597

Hellier, J.L., and F.E. Dudek. 2005. Chemoconvulsant model of chronic spontaneous seizures. *Curr. Protoc. Neurosci.* Chapter 9:19.

Hirai, S., A. Kawaguchi, J. Suenaga, M. Ono, D.F. Cui, and S. Ohno. 2005. Expression of MUK/DLK/ZPK, an activator of the JNK pathway, in the nervous systems of the developing mouse embryo. *Gene Expr. Patterns.* 5:517–523. http://dx.doi.org/10.1016/j.modgep.2004.12.002

Hirai, S., F. Cui, T. Miyata, M. Ogawa, H. Kiyonari, Y. Suda, S. Aizawa, Y. Banba, and S. Ohno. 2006. The c-Jun N-terminal kinase activator dual leucine zipper kinase regulates axon growth and neuronal migration in the developing cerebral cortex. *J. Neurosci.* 26:11992–12002. http://dx.doi.org/10.1523/JNEUROSCI.2272-06.2006

Holtmaat, A.J., J.T. Trachtenberg, L. Wilbrecht, G.M. Shepherd, X. Zhang, G.W. Knott, and K. Svoboda. 2005. Transient and persistent dendritic spines in the neocortex in vivo. *Neuron.* 45:279–291. http://dx.doi.org/10.1016/j.neuron.2005.01.003

Hunot, S., M. Vila, P. Teismann, R.J. Davis, E.C. Hirsch, S. Przedborski, P. Rakic, and R.A. Flavell. 2004. JNK-mediated induction of cyclooxygenase 2 is required for neurodegeneration in a mouse model of Parkinson's disease. *Proc. Natl. Acad. Sci. USA.* 101:665–670. http://dx.doi.org/10.1073/pnas.0307453101

Huntwork-Rodriguez, S., B. Wang, T. Watkins, A.S. Ghosh, C.D. Pozniak, D. Bustos, K. Newton, D.S. Kirkpatrick, and J.W. Lewcock. 2013. JNK-mediated phosphorylation of DLK suppresses its ubiquitination to promote neuronal apoptosis. *J. Cell Biol.* 202:747–763. http://dx.doi.org/10.1083/jcb.201303066

Jordan, B.A., B.D. Fernholz, M. Boussac, C. Xu, G. Grigorean, E.B. Ziff, and T.A. Neubert. 2004. Identification and verification of novel rodent postsynaptic density proteins. *Mol. Cell. Proteomics.* 3:857–871. http://dx.doi.org/10.1074/mcp.M400045-MCP200

Kelkar, N., S. Gupta, M. Dickens, and R.J. Davis. 2000. Interaction of a mitogen-activated protein kinase signaling module with the neuronal protein JIP3. *Mol. Cell. Biol.* 20:1030–1043. http://dx.doi.org/10.1128/MCB.20.3.1030-1043.2000

Kim, J.H., D. Liao, L.F. Lau, and R.L. Huganir. 1998. SynGAP: a synaptic RasGAP that associates with the PSD-95/SAP90 protein family. *Neuron.* 20:683–691. http://dx.doi.org/10.1016/S0896-6273(00)81008-9

Kuan, C.Y., A.J. Whitmarsh, D.D. Yang, G. Liao, A.J. Schloemer, C. Dong, J. Bao, K.J. Banasiak, G.G. Haddad, R.A. Flavell, et al. 2003. A critical role of neural-specific JNK3 for ischemic apoptosis. *Proc. Natl. Acad. Sci. USA.* 100:15184–15189. http://dx.doi.org/10.1073/pnas.2336254100

Lau, A., and M. Tymianski. 2010. Glutamate receptors, neurotoxicity and neurodegeneration. *Pflugers Arch.* 460:525–542. http://dx.doi.org/10.1007/s00424-010-0809-1

Lewcock, J.W., N. Genoud, K. Lettieri, and S.L. Pfaff. 2007. The ubiquitin ligase Phr1 regulates axon outgrowth through modulation of microtubule dynamics. *Neuron.* 56:604–620. http://dx.doi.org/10.1016/j.neuron.2007.09.009

Li, K.W., M.P. Hornshaw, R.C. Van Der Schors, R. Watson, S. Tate, B. Casetta, C.R. Jimenez, Y. Gouwenberg, E.D. Gundelfinger, K.H. Smalla, and A.B. Smit. 2004. Proteomics analysis of rat brain postsynaptic density. Implications of the diverse protein functional groups for the

integration of synaptic physiology. *J. Biol. Chem.* 279:987–1002. http://dx.doi.org/10.1074/jbc.M303116200

Mandir, A.S., M.F. Poitras, A.R. Berliner, W.J. Herring, D.B. Guastella, A. Feldman, G.G. Poirier, Z.Q. Wang, T.M. Dawson, and V.L. Dawson. 2000. NMDA but not non-NMDA excitotoxicity is mediated by Poly(ADP-ribose) polymerase. *J. Neurosci.* 20:8005–8011.

Mata, M., S.E. Merritt, G. Fan, G.G. Yu, and L.B. Holzman. 1996. Characterization of dual leucine zipper-bearing kinase, a mixed lineage kinase present in synaptic terminals whose phosphorylation state is regulated by membrane depolarization via calcineurin. *J. Biol. Chem.* 271:16888–16896. http://dx.doi.org/10.1074/jbc.271.28.16888

McLin, J.P., and O. Steward. 2006. Comparison of seizure phenotype and neurodegeneration induced by systemic kainic acid in inbred, outbred, and hybrid mouse strains. *Eur. J. Neurosci.* 24:2191–2202. http://dx.doi.org/10.1111/j.1460-9568.2006.05111.x

Migaud, M., P. Charlesworth, M. Dempster, L.C. Webster, A.M. Watabe, M. Makhinson, Y. He, M.F. Ramsay, R.G. Morris, J.H. Morrison, et al. 1998. Enhanced long-term potentiation and impaired learning in mice with mutant postsynaptic density-95 protein. *Nature.* 396:433–439. http://dx.doi.org/10.1038/24790

Miller, B.R., C. Press, R.W. Daniels, Y. Sasaki, J. Milbrandt, and A. DiAntonio. 2009. A dual leucine kinase-dependent axon self-destruction program promotes Wallerian degeneration. *Nat. Neurosci.* 12:387–389. http://dx.doi.org/10.1038/nn.2290

Morishima, Y., Y. Gotoh, J. Zieg, T. Barrett, H. Takano, R. Flavell, R.J. Davis, Y. Shirasaki, and M.E. Greenberg. 2001. Beta-amyloid induces neuronal apoptosis via a mechanism that involves the c-Jun N-terminal kinase pathway and the induction of Fas ligand. *J. Neurosci.* 21:7551–7560.

Muir, K.W. 2006. Glutamate-based therapeutic approaches: clinical trials with NMDA antagonists. *Curr. Opin. Pharmacol.* 6:53–60. http://dx.doi.org/10.1016/j.coph.2005.12.002

Murai, K.K., D. Misner, and B. Ranscht. 2002. Contactin supports synaptic plasticity associated with hippocampal long-term depression but not potentiation. *Curr. Biol.* 12:181–190. http://dx.doi.org/10.1016/S0960-9822(02)00680-2

Papouin, T., L. Ladépêche, J. Ruel, S. Sacchi, M. Labasque, M. Hanini, L. Groc, L. Pollegioni, J.P. Mothet, and S.H. Oliet. 2012. Synaptic and extrasynaptic NMDA receptors are gated by different endogenous coagonists. *Cell.* 150:633–646. http://dx.doi.org/10.1016/j.cell.2012.06.029

Peng, J., M.J. Kim, D. Cheng, D.M. Duong, S.P. Gygi, and M. Sheng. 2004. Semiquantitative proteomic analysis of rat forebrain postsynaptic density fractions by mass spectrometry. *J. Biol. Chem.* 279:21003–21011. http://dx.doi.org/10.1074/jbc.M400103200

Saito, T., and N. Nakatsuji. 2001. Efficient gene transfer into the embryonic mouse brain using in vivo electroporation. *Dev. Biol.* 240:237–246. http://dx.doi.org/10.1006/dbio.2001.0439

Sampedro, M.N., C.M. Bussineau, and C.W. Cotman. 1981. Postsynaptic density antigens: preparation and characterization of an antiserum against postsynaptic densities. *J. Cell Biol.* 90:675–686. http://dx.doi.org/10.1083/jcb.90.3.675

Saporito, M.S., E.M. Brown, M.S. Miller, and S. Carswell. 1999. CEP-1347/KT-7515, an inhibitor of c-jun N-terminal kinase activation, attenuates the 1-methyl-4-phenyl tetrahydropyridine-mediated loss of nigrostriatal dopaminergic neurons In vivo. *J. Pharmacol. Exp. Ther.* 288:421–427.

Schmued, L.C., C. Albertson, and W. Slikker Jr. 1997. Fluoro-Jade: a novel fluorochrome for the sensitive and reliable histochemical localization of neuronal degeneration. *Brain Res.* 751:37–46. http://dx.doi.org/10.1016/S0006-8993(96)01387-X

Sheng, M., and E. Kim. 2011. The postsynaptic organization of synapses. *Cold Spring Harb. Perspect. Biol.* 3:a005678. http://dx.doi.org/10.1101/cshperspect.a005678

Sherrin, T., T. Blank, C. Hippel, M. Rayner, R.J. Davis, and C. Todorovic. 2010. Hippocampal c-Jun-N-terminal kinases serve as negative regulators of associative learning. *J. Neurosci.* 30:13348–13361. http://dx.doi.org/10.1523/JNEUROSCI.3492-10.2010

Shin, J.E., Y. Cho, B. Beirowski, J. Milbrandt, V. Cavalli, and A. DiAntonio. 2012. Dual leucine zipper kinase is required for retrograde injury signaling and axonal regeneration. *Neuron.* 74:1015–1022. http://dx.doi.org/10.1016/j.neuron.2012.04.028

Simon, R.P., J.H. Swan, T. Griffiths, and B.S. Meldrum. 1984. Blockade of N-methyl-D-aspartate receptors may protect against ischemic damage in the brain. *Science.* 226:850–852. http://dx.doi.org/10.1126/science.6093256

Snider, B.J., F.J. Gottron, and D.W. Choi. 1999. Apoptosis and necrosis in cerebrovascular disease. *Ann. N. Y. Acad. Sci.* 893:243–253. http://dx.doi.org/10.1111/j.1749-6632.1999.tb07829.x

Tararuk, T., N. Ostman, W. Li, B. Björkblom, A. Padzik, J. Zdrojewska, V. Hongisto, T. Herdegen, W. Konopka, M.J. Courtney, and E.T. Coffey. 2006. JNK1 phosphorylation of SCG10 determines microtubule dynamics and axodendritic length. *J. Cell Biol.* 173:265–277. http://dx.doi.org/10.1083/jcb.200511055

Thakur, A., X. Wang, S.L. Siedlak, G. Perry, M.A. Smith, and X. Zhu. 2007. c-Jun phosphorylation in Alzheimer disease. *J. Neurosci. Res.* 85:1668–1673. http://dx.doi.org/10.1002/jnr.21298

Virgili, M., P. Migani, A. Contestabile, and O. Barnabei. 1992. Protection from kainic acid neuropathological syndrome by NMDA receptor antagonists: effect of MK-801 and CGP 39551 on neurotransmitter and glial markers. *Neuropharmacology.* 31:469–474. http://dx.doi.org/10.1016/0028-3908(92)90085-4

Waetzig, V., and T. Herdegen. 2005. Context-specific inhibition of JNKs: overcoming the dilemma of protection and damage. *Trends Pharmacol. Sci.* 26:455–461.

Walikonis, R.S., O.N. Jensen, M. Mann, D.W. Provance Jr., J.A. Mercer, and M.B. Kennedy. 2000. Identification of proteins in the postsynaptic density fraction by mass spectrometry. *J. Neurosci.* 20:4069–4080.

Watkins, T.A., B. Wang, S. Huntwork-Rodriguez, J. Yang, Z. Jiang, J. Eastham-Anderson, Z. Modrusan, J.S. Kaminker, M. Tessier-Lavigne, and J.W. Lewcock. 2013. DLK initiates a transcriptional program that couples apoptotic and regenerative responses to axonal injury. *Proc. Natl. Acad. Sci. USA.* 110:4039–4044. http://dx.doi.org/10.1073/pnas.1211074110

Xiong, X., X. Wang, R. Ewanek, P. Bhat, A. Diantonio, and C.A. Collins. 2010. Protein turnover of the Wallenda/DLK kinase regulates a retrograde response to axonal injury. *J. Cell Biol.* 191:211–223. http://dx.doi.org/10.1083/jcb.201006039

Yang, D.D., C.Y. Kuan, A.J. Whitmarsh, M. Rincón, T.S. Zheng, R.J. Davis, P. Rakic, and R.A. Flavell. 1997. Absence of excitotoxicity-induced apoptosis in the hippocampus of mice lacking the Jnk3 gene. *Nature.* 389:865–870. http://dx.doi.org/10.1038/39899

Yoshimura, Y., Y. Yamauchi, T. Shinkawa, M. Taoka, H. Donai, N. Takahashi, T. Isobe, and T. Yamauchi. 2004. Molecular constituents of the postsynaptic density fraction revealed by proteomic analysis using multidimensional liquid chromatography-tandem mass spectrometry. *J. Neurochem.* 88:759–768. http://dx.doi.org/10.1046/j.1471-4159.2003.02136.x

Zhu, Y., D. Pak, Y. Qin, S.G. McCormack, M.J. Kim, J.P. Baumgart, V. Velamoor, Y.P. Auberson, P. Osten, L. van Aelst, et al. 2005. Rap2-JNK removes synaptic AMPA receptors during depotentiation. *Neuron.* 46:905–916. http://dx.doi.org/10.1016/j.neuron.2005.04.037

Zuo, Y., A. Lin, P. Chang, and W.B. Gan. 2005. Development of long-term dendritic spine stability in diverse regions of cerebral cortex. *Neuron.* 46:181–189. http://dx.doi.org/10.1016/j.neuron.2005.04.001